AN INVESTIGATION AND EVALUATION OF PLASMA-SPRAYED CERAMICS FOR USE AS SPACECRAFT THERMAL CONTROL SURFACES

by

Robert J. Fenolia

ARTHUR LAKES LIBRARY
COLORADO SCHOOL OF MINES
GOLDEN, CO 80401

ProQuest Number: 10783928

All rights reserved

INFORMATION TO ALL USERS
The quality of this reproduction is dependent upon the quality of the copy submitted.

In the unlikely event that the author did not send a complete manuscript
and there are missing pages, these will be noted. Also, if material had to be removed,
a note will indicate the deletion.

ProQuest 10783928

Published by ProQuest LLC (2018). Copyright of the Dissertation is held by the Author.

All rights reserved.
This work is protected against unauthorized copying under Title 17, United States Code
Microform Edition © ProQuest LLC.

ProQuest LLC.
789 East Eisenhower Parkway
P.O. Box 1346
Ann Arbor, MI 48106 – 1346

T-4438

A thesis submitted to the Faculty and Board of Trustees of the Colorado School of Mines in partial fulfillment of the requirements for the degree of Master of Science (Materials Science).

Golden, Colorado

Date 3/26/96

Signed: _____
Robert J. Fenolia

Signed: _____
Dr. Dennis W. Readey
Thesis Advisor

Golden, Colorado

Date 3/26/96

_____
Dr. John J. Moore
Director,
Materials Science Program

ABSTRACT

Current aerospace manufacturing technology utilizes well-characterized organic, inorganic and silicone-based binders with ceramic oxide pigmentation for white coatings in order to meet thermal design requirements. These white coatings must be able to withstand the natural space environment without significant optical property degradation as well as being vacuum compatible in this intense radiation environment.

The research presented investigates and evaluates the use of plasma-spray ceramic as an alternative thermal control coating. Optimization of the plasma-spray process using a sodium aluminate powder, Cerametec BA200, was performed to achieve low solar absorptivity coatings. Simulated natural space environment testing of ultraviolet and electron irradiation was performed to characterize optical property degradation of BA200 plasma-sprayed coatings. Doping of the BA200 powder with Ce_2O_3 was performed, to inhibit optical property degradation, and the resultant plasma-sprayed coating was subjected to ultraviolet and electron irradiation.

Optical property characterization, limited physical property characterization, and simulated space environment exposures were performed on plasma-sprayed BA200 coatings to show their viability as spacecraft thermal control coatings.

TABLE OF CONTENTS

Page

LIST OF FIGURES

LIST OF TABLES

Page

ACKNOWLEDGMENTS

A special appreciation to Mr. Ed Pierson for his dedicated support and to Lockheed Martin Corporation for allowing this research to be possible.

DEDICATION

This thesis is dedicated to my loving wife, Char, and to my children, Nichole, Jake, and Levi who have sacrificed and endured my efforts.

1. INTRODUCTION

1.1 Purpose

The purpose of this thesis is to investigate white spacecraft thermal control coatings and the use of more beneficial modern coating technologies to produce new coatings for this application. Plasma-sprayed white ceramic oxide coatings were investigated to satisfy the criteria for use as spacecraft thermal control coatings.

Literature reviews were conducted to examine previous research of white thermal control coatings intended for or used as spacecraft surfaces. Additionally, literature reviews for plasma-sprayed white oxide coatings were conducted. Many types of coating are used for this type of application. These techniques, and their resultant coatings, were investigated. The beneficial and detrimental aspects of these coatings as spacecraft thermal control coatings were compared.

1.2 Thermal Control Balance of Spacecraft Surfaces

Spacecraft thermal balance depends on the optical properties of the exterior surfaces. For solar-facing spacecraft surfaces, it is desirable to have a very low ratio of solar absorptivity to hemispherical emittance (α_s/ε_h) in order to keep spacecraft hardware and component surface temperatures within qualification and design parameters.[1] Solar absorptivity (α_s) is the radiation absorbed by a material from the solar spectrum (0.25μm to 2.5μm). Thermal

emissivity, typically measured as hemispherical emittance (ε_h) is the reflectance by a material in the infrared wavelength region (2.5μm to ~50μm). Current aerospace manufacturing technology utilizes well-characterized organic, inorganic and silicone-based binders with ceramic oxide pigmentation for white coatings in order to meet thermal design requirements.[1, 2, 3, 4, 5, 6, 7] White coatings typically have a solar absorptivity from 0.15 to 0.3 and a thermal emittance of greater than 0.8. These white coatings must be able to withstand the natural space environment without significant optical property degradation as well as being vacuum compatible in this intense radiation environment.[8]

Current thermal design methods for sizing passive radiators utilize end-of-life, degraded coating optical properties. [1] Optical properties of existing white thermal control coatings have been extensively investigated. [1, 2, 3, 4, 5, 6, 7] Significant coating optical property degradation, as observed by end-of-life optical properties, is mainly due to exposure to the natural space environment. [8] This results in the design of larger radiator surfaces in order to keep components cool. Accordingly, increases in the weight, bulk, and cost of the resulting spacecraft are encountered. In addition, some passive thermal design components must use actively-heated devices during the initial flight until the thermal control surfaces have reached a degraded value. This factor complicates the tasks of the thermal control design engineer.

Room-temperature thermal radiators are generally planar structures whose area is sized to reject the dissipated heat under worst-case environment (orbit and spacecraft orientation) and load profiles.[9] First-order orbital average sizing methods neglect the dynamics of the orbital environment as well as the spacecraft response, but are often accurate enough for preliminary designs. In such analyses, the required radiator area is linearly proportional to the average

heat rejected by the payload plus the average heat absorbed from environmental sources. For initial sizing efforts, the assumption used is that the radiator area is proportional to the fourth power of average radiator temperature times the infrared emissivity. The absorbed heat load is divided into two parts; that absorbed in the visible wavelengths (α_s) from direct solar incidence as well as sunlight reflected from the Earth (albedo) and from other spacecraft surfaces, and that absorbed in the infrared wavelengths (measured as hemispherical emittance, ε_h) from sources such as Earth reradiation and views to other warm spacecraft surfaces. For sizing purposes, the use of an effective environmental "sink temperature" is a mathematical convenience that helps intuitive understanding. Sink temperatures in low-Earth orbit (LEO) typically range from -150°C to 50°C, and orbital average sink temperatures are usually within the range of -80°C to -20°C. The closer the radiator temperature is to the sink temperature, the larger the required heat transfer area. Because the sink temperature is mostly a function of absorbed heat from exposed spacecraft surfaces, it is dominated by the value of α_s for radiators that operate at or below room temperatures. Low end-of-life solar absorptivity is the single most important parameter in radiator sizing at room temperatures and below.[1]

The thermal characteristics of cryogenic radiators and their related baffles and shields impose demanding requirements on coating technology for conventional missions. Typical sensor cooling applications use multi-stage cryogenic radiators (or shields) to achieve temperatures in the range of 40 K to 150 K.[9]

The low temperature applications (~ 40 K to 100 K) never allow direct or Earth-reflected (albedo) solar flux to directly impinge on the coldest stage. The resulting heat gain with a solar absorptance of 0.02 to 0.10 would totally

overwhelm the ability of the radiator to hold its low temperature. Hence, the typical design approach with these radiators is to maximize the surface emittance and eliminate environmental radiative inputs (Earth IR, spacecraft surface views, albedo and direct solar) by extensive shielding schemes.

For higher temperature radiators (or warmer stages in multi-stage radiators), the design may require a very low solar absorptance and a high thermal emittance. Typical materials include second-surface devices such as thin glass mirrors or plastic films that are aluminized (or silverized) on the interior side. These devices typically achieve solar absorptivities in the range of 0.05 to 0.09 (beginning of life or initial, unexposed to the space environment solar absorptivity values). Thermal emissivities for these materials are typically 0.75 to 0.80.

Low-end stable solar absorptivity can be enabling technology for certain missions since there are practical limits to the size of a radiator. A spacecraft has only a limited amount of available area for body-mounted radiators.

In preliminary design studies, radiator weight is usually assessed as a linear function of area, typically 5 kg/m^2 for normal applications. However, the support structure required to withstand launch vibrations and acoustic environments generally make the total weight rise nonlinearly. Thus, a 5% reduction in area will generate more than 5% weight savings. The selection of a radiator thermal control coating material can be a factor in this weight reduction.

1.3 Optical Property Stability

The optical stability of a thermal control radiator coating surface must be demonstrated for each of the natural space environments. The reaction and degradation of each environment must be minimized, since changes caused by one environment can accelerate the degradation of another.

The optical properties of radiator surfaces are critical parameters necessary for establishing the performance of a material in meeting operational and system requirements. These properties are defined by the material solar absorptance (α_s) and hemispherical emittance (ε_h). The ratio of solar absorptance to hemispherical emittance (α_s/ε_h) will directly define the radiator area and orbital average sink temperature required to meet certain system operational temperature requirements. The beginning-of-life (BOL) radiator optical properties can have a significant influence on system radiator size and weight that ultimately affect system cost.[9] The reproducibility of the initial optical properties for spacecraft coatings is also very important since this establishes the confidence level the thermal control engineer uses for design. This, combined with degraded end-of-life (EOL) optical properties, ultimately determines the final radiator size. This interrelationship of how optical properties can effect the radiator size is shown graphically in Figure 1.

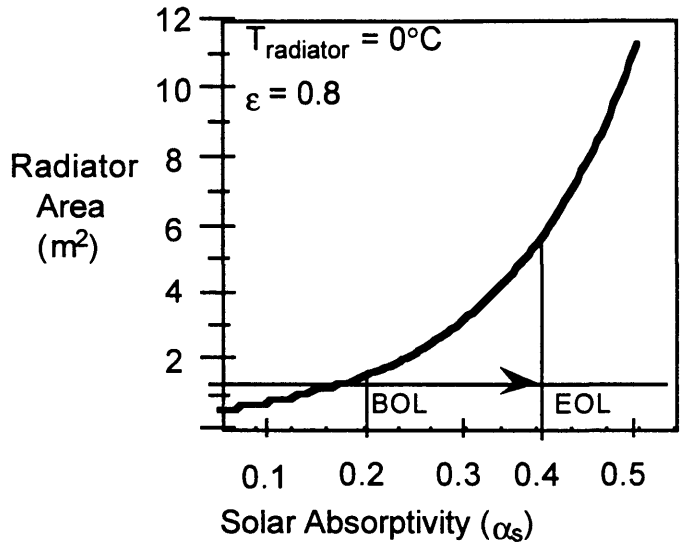

Figure 1 Optical Property Influence on Radiator Size

1.4 Natural Space Environment

The natural space environment consists of solar ultraviolet radiation, charged particles, atomic oxygen molecules, and extreme vacuum conditions.[10,11] The specific environmental conditions a spacecraft is subjected to are dependent on orbit parameters (altitude, inclination, etc.) and mission duration. Survivability of spacecraft thermal control surfaces are dependent on these specific environmental conditions.

The solar UV radiation environment is one of the most stressing for thermal control surfaces. UV radiation is comprised of a solar irradiance spectrum of 0.135 W/cm^2 with radiation below a wavelength of 0.4 μm. The spectrum consists of a far UV (FUV) region, 0.115 to 0.180 μm, and a near UV (NUV) region, 0.190 to 0.40 μm. The interaction of the UV radiation with thermal control coating materials can result in optical property changes that arise from

the production of free carriers and/or excited atoms.[12] The presence of free carriers is manifested by free-carrier absorption and by luminescence that results from radiative recombination or de-excitation of trapped charges or excited atoms.[12] The latter species can also result in a transient absorption.[12]

The effects of charged particles (electrons, e^-, and protons, p^+) on spacecraft materials have been demonstrated by numerous space flight experiments to degrade the optical properties of thermal control coatings.[13] The electron environment is composed of high-energy geomagnetically-trapped (Van Allen belt) electrons and low-energy electrons. Coating damage and degradation are induced from large fluences of lower energy electrons that cause ionization, excitation, and free radical formation rather than the displacements more closely associated with higher energy electrons. The proton environment is divided into three groups: plasma-sheet protons, geomagnetically-trapped (radiation belt) protons, and solar flare protons. For thermal control coatings, the plasma-sheet protons have been determined to be far more damaging to material surfaces. [12] In calculating and simulating the effects of charged particles on spacecraft surfaces, it is essential to determine the energy spectra and the time-integrated particle flux of the particles.

In a geosynchronus Earth orbit (GEO), a spacecraft will encounter low-energy plasma sheet electrons (1 to 20 keV) and protons (10 to 50 keV), as well as higher energy protons (>100 keV). In lower orbits, a spacecraft will see trapped radiation of higher energies, 3-keV to 7-MeV electrons and 15-keV to 1000-MeV protons.

The atomic oxygen (AO) environment, formed by the dissociation of O_2 by UV radiation, is present in the Earth's ionosphere at orbital altitudes of 200 to 700 km and higher. The reactivity of AO is recognized as a serious threat to

thermal control radiator coatings exposed to its orbital ram flow, since material erosion or optical property degradation may occur. The motion of the spacecraft through the residual atmosphere in low-Earth orbit (LEO) at velocities of 7.5 to 8 km/s results in an equivalent impingement energy for AO of 4.5 to 5.0 eV.

Simulations of these natural space environments are necessary to determine optical and thermophysical property degradation of thermal control coatings.[9] On-orbit thermal cycling, solar ultraviolet (UV) radiation (far UV and near UV), low-energy protons and electrons, and atomic oxygen (AO) are the predominant natural environment components that can cause surface property changes and optical property degradation.[9] Stability in the natural space environments is of prime importance, since degradation can lead to subsystem or mission failure. Spacecraft coating materials are most susceptible to damage from the lowest energy particles, and simulated testing environments should be consistent with the these levels.[12]

1.5 Space Stability of Thermal Control Coatings

The natural space environment radiation can produce extensive optical property degradation to spacecraft coatings. White thermal control coatings are especially critical surfaces since optical property degradation can induce a spacecraft thermal imbalance. The radiation damage in white thermal control coatings results in solar absorptivity (α_s) degradation that is manifested by the formation of optical absorption bands (color centers) in the UV-visible spectrum not present in the virgin material. Understanding the basic mechanisms influencing the formation of these radiation-produced absorption bands in the UV-visible spectrum assists in the characterization efforts involved during coating development efforts.

Thermal control coatings tested for 5 years on spacecraft (ML-101 flown on STP P72-1 and SKYLAB D024), excluding contamination effects, optically degraded (due to the space environment radiation) according to Equation 1, [9]

$$\Delta\alpha_s = K\,t^n \qquad (1)$$

where $\Delta\alpha_s$ is the change of solar absorptivity observed, K is a constant, t is time, and the exponent n is less than 1. Both K and n are material dependent.[9] The usefulness of white thermal control coatings on spacecraft is dependent on the degree of radiation damage observed in the thermal control coating and the ability to understand and characterize these radiation-induced effects.

Optical property degradation occurs in both organic (including silicones) and inorganic-based white thermal control coatings and results from intrinsic defects of the metal oxide pigments used in these coating systems.[14] Intrinsic (native) defects (vacancies, impurities, interstitials, free electrons, and holes) are inherent in inorganic compounds and arise from lattice stability and thermodynamic reasons. Radiation damage in materials results in the formation of electronic defects (free electrons and holes), by ionization or partial ionization (exciton behavior) from the radiation exposure, which then combine with the intrinsic defects resulting in color centers.

An example of this can be explained as follows: oxygen bleaching (or photodesorption) is well referenced in literature[2, 14] as a mechanism resulting in α_s degradation in metal oxide pigment white thermal control coatings. This process involves a metal oxide becoming nonstoichiometric which is represented by the following reversible point defect reaction shown in Equation 2;

$$O_0 \overset{h\nu}{\Leftrightarrow} \frac{1}{2} O_2\,(g) + V_0^{\bullet\bullet} + 2e' \qquad (2)$$

where O_0 is an oxygen atom on a normal oxygen lattice site, $V_0^{\bullet\bullet}$ is a vacant oxygen lattice site, e' is a free electron, and $\frac{1}{2}\ O_2\ (g)$ is gaseous oxygen, described using Kröger-Vink notation. From this reaction equation, the vacant oxygen site is proportional to the oxygen pressure and a function of the phonon (hν) flux. The reaction, at equilibrium, can be driven to the left or right, depending on the oxygen pressure. The reaction will reverse to the left (anneal) and return to the original state, if the radiation source is removed or the coating returned to an ambient environment. If, however, the vacant oxygen site or free electrons combine with other inherent defects associated in the host material that are more thermodynamically stable, a new absorption band, associated with this new combination, will result and persist.

The oxygen vacancy and free electron concentrations produced are also proportional to the oxygen pressure at equilibrium. These point defects (the vacant oxygen) and the electronic defects (free electrons) can combine with other intrinsic point defects (e.g., trace metal impurities, native Shottky or Frenkel defects) which will result in coloration. This also implies that the natural environment testing (UV, electron, or proton) should be performed in vacuum with in-situ α_s measurements to fully understand and quantify these effects.

Extrinsic impurity concentrations at levels as low as 10 parts-per-million (ppm) can result in color centers.[15] The impurity concentration will define the degree of coloration. For example, the coloration and different hues of the ruby gemstone arise from chromium impurities in alumina. Similarly, the coloration and different hues of emeralds arise from chromium impurities in beryllium silicate, and the coloration and different hues of sapphires arise from titanium impurities in alumina.

Point defect chemistry, which is the solid-state chemistry concerned with the formation and reactions of defects, is necessary in order to understand discolorations of thermal control coatings that occur during coating characterization efforts. This is the same technology used in ceramic engineering responsible for the development of high-temperature solid-state electrolytes used for oxygen sensors, fuel cells, oxygen pumps, and solid-state batteries, and for engineering semiconductor materials.

1.6 Research Overview

The emphasis of this research is to document the optical property degradation and mechanisms associated with several currently used white thermal control coatings. In addition, the use of plasma-sprayed white oxide coatings for future spacecraft applications will be explored and characterized for their optical property stability in a space radiation environment.

Literature surveys were performed to identify ceramic materials with high temperature stability (>1000°C) and appearing extremely white in their as-applied form. From this initial survey, plasma spraying techniques were identified to be the most promising technique to apply a variety of types of ceramic compound coatings to the substrates of interest. Numerous vendors were then contacted to produce plasma-sprayed coatings of these compounds on various substrates.

Initial investigations into the use of plasma-sprayed Al_2O_3 coatings exhibited promising resistance toward optical property degradation as demonstrated in simulated V-UV, e^-, and p^+ space environments. Investigation of plasma spray coating application variables was performed to optimize the

initial optical properties of the applied coatings using Al_2O_3 precursory powder materials. Dopant materials were investigated and selected to counteract the effects of color center formation in the resultant plasma-sprayed Al_2O_3 coatings. Doped Al_2O_3 powders were used to produce coating samples that were then subjected to simulated V-UV, e^- environments. Optical properties of these coatings, as well as other physical properties, are presented.

1.7 Plasma-Spraying Coating Process Overview

Plasma spraying allows ceramic materials to be deposited as coatings without the use of binders. This is important because these coatings exhibit superior durability, have higher use temperature capabilities, and show additional resistance to degradation in natural space environments compared with currently used spacecraft coatings.

During the plasma-spray coating deposition process, a powdered material (either ceramic or metallic) is suspended in a carrier gas that is injected into a DC-arc generated plasma. A schematic representation of the plasma gun is shown in Figure 2. The plasma-spray system components are listed in Table 1. The plasma enthalpy is controlled by adjusting the flow rates of high velocity gases. The primary gas (primary because it is the main contributor to the plasma enthalpy) and secondary gas flow rates are adjusted to provide the correct thermal and velocity environments for the deposition process. These flow rate parameters are typically recommended by the plasma-spray equipment manufacture or the plasma-spray powder manufacturer. The powder particles enter the plasma stream and are accelerated (at rates up to

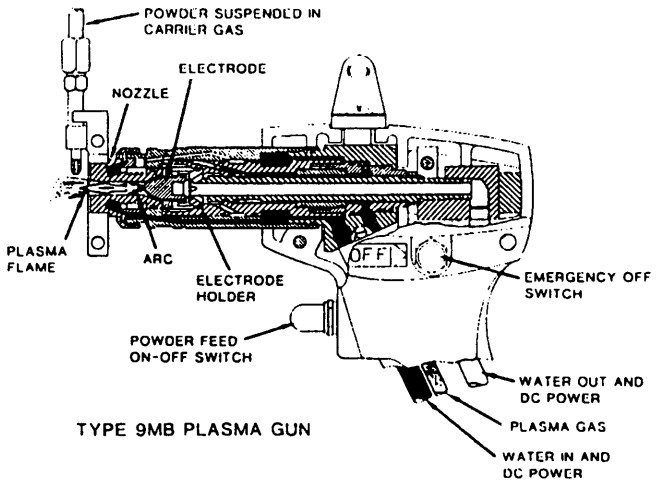

Figure 2 Metco 9MB Plasma Spray Gun[16]

Table 1 Metco Plasma Spray System Equipment

ITEM	Type #
Plasma Spray Gun	9MB-D 80kW
Plasma Control	7MC-II
Power Supply	8MR-230
High Frequency Unit	
Water to Water Heat Exchanger	8ME
Powder Hopper	4MP
Powder Feedrate Control	4MP-800
Spray Robot	AR2000
Cable And Hose Package	7MH, 7GH, 7GNR
Heat Exchanger Water Conditioning Chemical Element	8MK-811
Air Control Unit	5A

supersonic velocities) during which powder particles are melted, or partially melted, and deposited (splatted) on the substrate material. The powder particles solidify and form a coating layer. Numerous layers are deposited to produce the desired coating. Variables that affect the optical properties of the resultant coating must be controlled in this application process in order to give a repeatable, reliable process suitable for production manufacturing.

Initial plasma-sprayed coating evaluation efforts showed variations in the optical properties of coatings produced by different plasma spraying vendors with identical powder materials. As a result of these efforts, Lockheed Martin procured a plasma spray deposition system in order to develop these types of coatings for spacecraft thermal control coatings. The variations in the optical properties of the resultant thermal control coatings were evaluated by optimizing and controlling the plasma spraying deposition parameters.

In order to develop and qualify plasma-sprayed spacecraft thermal control coatings, there must be a thorough understanding of the starting powders and the plasma-spray deposition processes used to produce the coatings. In addition, the environments to which the coatings will be exposed to must be considered. With the understanding of the materials, processes, and environments, the coating application technique can be optimized to isolate and minimize the effects of variables that intrinsically affect the resultant coating's chemistry, crystalline structure, and morphology.

The starting ceramic oxide powder chemistry and crystalline structure can be adversely altered during the plasma-spray process.[17] Exact control of the starting powder chemistry and particle size distribution could be meaningless if the operating parameters of plasma deposition introduce elemental contamination, or cause undesirable phase transformation. For

these reasons, consideration must be given to both the starting material's chemistry and the plasma deposition environment, when attempting to optimize the coating deposition parameters. In addition, the substrate can also affect the coating morphology and adhesion during deposition. Coating morphology is dependent on the temperature during deposition and during solidification (cooling of the particles) when deposited on the substrate surface.[16] Different substrate materials possess thermal conductivities and specific heats that allow the coating solidification and cooling rates to be different. Therefore, when optimizing a thermal control coating, all variables must be carefully considered in order to control as many of the variables as possible during the thermal control coating application.

2. BACKGROUND AND THEORY

2.1 Degradation of Thermal Control Coatings

2.1.1 Physical Degradation

Degradation in the solar absorptivity of white thermal control coatings has been a common concern with satellite design for over twenty years.[10,18, 19, 20] A significant effort has been expended only to result in coatings which still exhibit slight degradation of optical properties when exposed to the extremes of the natural space environment.[10, 18, 19, 20] Table 2 lists the most commonly used spacecraft white thermal control coatings and which will be further discussed in this thesis. The coatings shown in Table 2 comprise the majority of the materials used for all spacecraft white thermal control coating applications and have been well characterized regarding optical property degradation in the natural space environment.[10, 18, 19, 20] A brief description of these coatings is given in the following paragraphs.

A276: Chemglaze A276 is a proprietary urethane based coating manufactured by Lord Products. The A276 coating uses a titanium dioxide pigment dispersed in a urethane binder system. The coating system consists of four parts (base, hardener, flattener, and additive) which are mixed together prior to coating application. The coating is applied using conventional air spray techniques and cures for 14 days at room temperature.

ARTHUR LAKES LIBRARY
COLORADO SCHOOL OF MINES
GOLDEN, CO 80401

Table 2 White Coatings Used for Spacecraft Surfaces

Designation	Pigment	Binder	Manufacturer	Reference
A276	TiO_2	Polyurethane	Lord	18
S13G	ZnO	Silicone	IITRI	
S13G\LO	ZnO	Silicone	IITRI	18
92-007	TiO_2	Silicone	Dow Corning	10, 19
YB-71	ZOT	K_2SiO_4	IITRI	20
Z93	ZnO	K_2SiO_4	IITRI	19
MS74	ZnO, Al_2O_3, TiO_2	K_2SiO_4	NASA	

ZOT - Zinc Orthotitanate

S13G: The S13G coating manufactured by IITRI uses a zinc oxide pigment dispersed in an elastomeric silicone binder. The zinc oxide (SP500 from New Jersey Zinc Co.) has a purity of 99.90% with a mean particle size of 0.25 to 0.35 μm. The zinc oxide pigment is dispersed into a silicone elastomer binder (RTV602 from General Electric). The coating is applied using conventional air spray techniques and cures for 7 days at room temperature.

S13G\LO-1: The S13G\LO-1 coating uses a reactively encapsulated zinc oxide pigment dispersed in an elastomeric silicone binder. This coating is a hybrid of the Z93 (pigment) and the S13 coating. IITRI developed a process that uses potassium silicate to reactively encapsulate the zinc oxide pigment. The reactive encapsulation of the zinc oxide pigment was shown to inhibit UV caused degradation. In this process the zinc oxide is first reacted in a slurry with the potassium silicate. The encapsulated particles are extracted and dried prior to being milled with the silicone elastomer binder (V-10 from General Electric). The pigment is combined with the binder in a 2:1 ratio by weight. The coating is applied using conventional air spray techniques and cures for 7 days at room temperature.

92-007: The 92-007 coating manufactured by Dow Corning uses a titanium dioxide pigment dispersed in an elastomeric silicone binder. The coating is applied using conventional air spray techniques and cures for 7 to 14 days at room temperature.

YB71: The YB71 coating uses a zinc-orthotitanate ($ZnTiO_4$, ZOT) pigment dispersed in a potassium silicate binder. The ZOT is synthesized by a calcination of zinc oxide and titanium oxide precursor powders. The calcination process results in a very fine ZOT powder, requiring no further grinding or crushing, suitable for use as a pigment. . The ZOT pigment is dispersed into the potassium silicate (PS7 from Sylvania) and thinned with deionized water in the ratio of 7:1:1 by weight (pigment:binder:water). The higher pigment loading, as compared to the Z93 and S13G/LO coatings, results in a higher solar reflectance in the UV region. The higher pigment ratio also results in increased stability due to the decreased amount of the silicate binder in the coating that is partially responsible for the coating's degradation. These aspects of degradation will be discussed later in this thesis. The YB71 coating was developed after the Z93 and S13 G/LO coatings to provide additional stability in UV, e-, and p+ space environments. The coating is applied using conventional air spray techniques and cures for 14 days at room temperature.

Z93: The Z93 coating manufactured by IITRI uses a zinc oxide pigment dispersed in a potassium silicate binder. The zinc oxide (SP500 from New Jersey Zinc Co.) has a purity of 99.90% with a mean particle size of 0.25 to 0.35 μm. The zinc oxide pigment is dispersed into the potassium silicate (PS7 from Sylvania) and thinned with deionized water in the ratio of 4:3:1 by weight (pigment:binder:water). The coating is applied using conventional air spray techniques and cures for 7 days at room temperature.

MS-74: MS-74 was developed and is manufactured by NASA, Goddard Space Flight Center. The MS-74 coating uses three pigment materials that are milled together in the ratio by total coating weight of; 16% zinc oxide (SP500 from New Jersey Zinc), 11% aluminum oxide (Linde C from Union Carbide Corporation), and 16% titanium dioxide (RF-1 from New Jersey Zinc). The pigments are then dispersed in potassium silicate (PS7 from Sylvania) and potassium hydroxide (Fisher Scientific) binder. The binder constitutes 57% by weight of the coating material. The coating is applied using conventional air spray techniques and cures for 7 days at room temperature.

Table 3 shows initial and end-of-life optical property data obtained from flight and simulation experiments with some of these coatings. These data show typical optical property degradation resulting from exposure to the natural space environment.

Some of the coatings shown in Table 2 (specifically those with inorganic binders) are very sensitive to handling and contamination that can occur during manufacturing and pre launch activities. Inorganic binder coatings are typically vacuum stable but, due to the high pigment concentration needed to develop optical properties, these coatings have a chalky finish that easily spalls small particles that can contaminate other spacecraft surfaces. Organic binder coatings typically have outgassing products that can contaminate sensitive optical surfaces when used in thermal vacuum environments. In addition these coatings can be easily marred or contaminated during manufacturing operations that lower their initial solar absorptivity. Silicone binder coatings

Table 3 Initial and Degraded Optical Properties of White Spacecraft Coatings

Coating	Initial α_s	Initial ε_h	1 year α_s	Flight Experiment / Simulation	Reference
A276	0.27	0.87	0.41***	Simulation	18
S13G\LO	0.18	0.91	0.25***	Simulation	18
92-007	0.19	0.87	0.33*	STP P72-1	10
92-007	0.24		0.34**	Apollo 9	19
YB-71	0.17		0.24	AESC Calorimeter	20
YB-71	0.18		0.28****	Geosynchronous orbit	6
Z93	0.16		0.29**	Simulation	

* - 5700 sun hours
** - end of mission
*** - 600 Equivalent Sun Hours
**** - 800 days

also have outgassing products that can be a contamination source when used in thermal vacuum environments. These coatings are relatively soft and are easily damaged during manufacturing operations.

It is the desire of the thermal control design engineer to use white coatings which posses a low solar absorptance to hemispherical emittance ratio (α_s/ε_h). Flight experimental data indicates that emittance properties of coatings do not degrade with time, therefore optical degradation of white thermal control coatings can solely be attributed to increases in the solar absorptivity.[20]

Solar absorptivity degradation of white thermal control coatings results from one or more (or combinations thereof) of the following mechanisms shown in Table 4. Contamination of thermal control surfaces leading to the optical property degradation has been know about since optical property experiments

Table 4 Solar Absorptivity Degradation Mechanisms of White Thermal Control Coatings

Contamination
Vacuum stability (outgassing products)
Micrometeoroid damage
Thermal cycling
Radiation effects (UV, electron, proton)
Chemical degradation (oxygen diffusion, atomic oxygen)

have flown aboard satellites. [19, 20] Molecular contamination results from the condensation of volatilized matter on the surface of the thermal control coating from the coating itself outgassing, or from other spacecraft materials outgassing. Molecular contamination of a thermal control coating decreases the coatings' reflectance and thereby increases the solar absorptance. Since the late 1960's, requirements for have low outgassing materials and enhanced manufacturing techniques significantly reduced molecular contamination levels to a point where contamination of the thermal control coating is no longer a primary concern. It is needless to say, that thermal control coating materials must still meet established spacecraft outgassing requirements. Vacuum baking techniques and tighter contamination control efforts have substantially reduced molecular contamination concerns for current satellite thermal control surfaces and need not be further discussed here. [This is supported by the satellite P78-2(SCATHA) which was flown in a 27.6 x 43.3 km geosynchronous orbit. SCATHA carried the ML12 experiment which contained sixteen thermal control materials (none of which were white coatings).] Contamination was eliminated as a source of the optical property degradation observed with these materials

and radiation damage (mainly UV, electron and proton) was suspected to cause the degradation observed.[13]

Micrometeoroids, particles with high kinetic energies and small mass, impact thermal control coatings during spacecraft missions and result in physical and mechanical damage. Thermal control coatings resistant to these impacts will reduce the physical damage of the thermal control coating as well as the spacecraft structure itself.

Thermal control coating damage resulting from thermal cycling arises from stress fatigue in the coating, and at the coating/substrate interface, resulting in coating cracking and adhesion failure. Thermal fatigue is a term denoting the effects of temperature changes or alternating exposure at higher and lower temperatures on the life or usefulness of a material. If the heating and cooling cycle stresses does not exceed the elastic limit of the material and plastic flow does not actually result, thermal fatigue will not generally occur. Generally, higher conductivity materials have a much better chance for survival since they distribute the heat much more evenly in a relatively short period of time. Thermal shock is due to the severity of the temperature rate change with time and results when the stresses exceed the tensile, and sometimes compressive, strength of the coating. It is necessary that the heat transfer coefficient be understood to predict thermal shock resistance properties. The differences between thermal fatigue and thermal shock failure are primarily related to the rate of change of temperature and the severity of the temperature gradient. High stresses, either residual or applied, are directly related to the mechanism of thermal fatigue or cycling failure. Stresses occur in coatings from (1) differential thermal expansion, (2) operational stresses, and (3) residual stresses from coating application processes. The latter two are generally resultant from the first.

Experimental data and studies of solid state chemical reactions have been extensively reported in the literature, but relatively few studies between the coating and substrate systems currently of interest have been performed.[14] For higher temperature applications, thermodynamic factors are the major criterion determining whether or not a reaction will occur and consideration and an understanding of the basic degradation mechanisms must be accounted for in the proper design of the coating system. Thermodynamic calculations can still lead to erroneous conclusions through the assumptions that the reactants are stoichiometric since a deviation from stoichiometry will have profound effects on the stability and properties of the coating.

2.1.2 Optical Degradation

The degradation mechanisms previously discussed (contamination, vacuum stability, micrometeoroid damage, and thermal cycling), although important, need not be discussed any further because they are generic in nature and apply to any thermal control coating. More importantly, the majority of degradation of optical properties experienced by thermal control coatings is caused by radiation effects and chemical degradation mechanisms.[14] These two mechanisms of degradation will be examined in more detail in the following sections. The emphasis of this thesis will focus upon the stability of these coatings towards these (radiation effects and chemical degradation) mechanisms.

Radiation damage from the natural space environment (arising mainly from UV, electrons (e^-), and protons (p^+)) cause discolorations of pigments and decomposition of binder material in current thermal control coatings.[14] These degradation mechanisms can involve color center formation, ionization, and

other chemical mechanisms leading to deterioration of the pigment and binder systems.[14] Chemical degradation is mainly centered around oxygen diffusion and photoreduction process and atomic oxygen damage. Residual oxygen in the pigment materials or the result of pigment or binder decomposition can result in additional defect mechanisms effecting the solar absorption. Atomic oxygen, a strong oxidizing agent, with high kinetic energy causes mechanical damage (mainly from erosion) and chemical damage to a thermal control coating.

In order to achieve a space-stable white thermal control coating, the basic mechanisms of each type of degradation must be understood, or at least considered, and reconsidered for combined effects mechanisms involving several degradation mechanisms. For the past decade, synergistic effects of degradation mechanisms have been recognized, but limited combined environmental testing has been performed on thermal control coating materials to attempt to understand the mechanisms of degradation.[21] More recently, concern over atomic oxygen degradation has been given considerable attention as a major cause of degradation and much effort has been expended to simulate this aggressive environment.[21] The majority of the combined environmental testing, when it has been performed, has been directed towards the concerns shown in Table 5.

Table 5 Combined Environments Testing Concerns

ultraviolet radiation stability
visible radiation stability
vacuum stability
optical property degradation (both in-situ and ex-situ)
atomic oxygen

Nearly 99% of the total space radiation energy is contained in the spectral region between 300nm to 4000nm. In the UV region below 140nm, there is considerable structure in the solar spectral distribution due to various emission lines of excited atoms.[12] Radiation due to particulate matter includes primarily the electron and proton flux. Proton energies above 40 MeV and electrons with energies above 20 KeV may be encountered arising from solar flare activities. On occasion a burst of protons with energies of a few BeV can also be encountered. In spacecraft applications, the UV portion of the solar spectrum causes the most damaging effects in coating materials. Metals are essentially unaffected, but nonmetals (including inorganics and ceramics) are susceptible. In polymeric systems, the liberation of gaseous products, dissociation of atomic bonds, and formation of free radicals are experienced. Silicate glasses tend to discolor and suffer transparency loss.

The solar reflectance of a white coating depends upon the coating's ability to scatter light in a very broad wavelength region. Light scattering theory has its origins in the Maxwell equations leads to the expression that relates the particle diameter to maximum scattering in the form:

$$d(\lambda) = \frac{0.90(m^2 + 2)}{n\pi (m^2 - 1)} \lambda \qquad (3)$$

where d is the particle diameter at which maximum scattering occurs for wavelength (λ), n is the refractive index of the medium surrounding the particle, and m is the ratio of the refractive index of the material in the particle to that of the medium.[2] Equation 3 shows how the particle size is related to optical reflectance and in addition, how a binder influences the reflectance properties of a coating.

2.2 Previously Observed Phenomena

The Illinois Institute of Technology and Research Institute (IITRI) has been known for their research and manufacturing of spacecraft coatings for several decades. The most prominent IITRI coatings (see Table 2)[9] have utilized zinc oxide and zinc orthotitanate ceramic pigments dispersed in inorganic (potassium silicate) and silicone binders. From spacecraft flight experiments with these coatings, as well as extensive research by IITRI, much has been learned regarding the radiation-induced chemical degradation mechanisms of the pigment materials when exposed to a space radiation environment. This research included morphological investigations comparing surface roughness and surface area of the zinc orthotitanate pigments with the ultraviolet radiation stability of coatings. One important result of these investigations indicated that the pigment surface area is directly related to the degradation mechanism of the solar absorptivity. This is shown by the relationship scattering reflectance and pigment particle size given in Equation 3.

During IITRI's investigations[2, 5, 22] emphasis was placed on the optical property stability of the coating, although studies of the individual components (binder and pigment) were required to establish the critical parameters. A correlation of the pigment particle morphology with optical property degradation was obtained in this research when examining existing coating materials. As a corollary, IITRI found that bleaching of the pigment by oxygen was further evidence of oxygen desorption during degradation.[14] Pigment encapsulation by the binder in the coating may be so poor (non continuous), that in high pigment concentrations, small air gaps can cause sharp increases in gas permeation rate that results in inconsistent degradation of coatings with

equivalent binder systems. This erratic degradation response of some coatings may be due to ineffective encapsulation of the pigment. For zinc oxide and zinc orthotitanate pigments, a reasonable correlation was found between solar absorptivity degradation by UV irradiation and the pigment particle morphology (surface roughness and surface area). This may be explained by the relationship of reflectance, particle surface area, and refractive index (influenced by the pigment encapsulation by the silicate binder for these coatings) previously described in Equation 3. If UV degradation is a surface controlled phenomena, then increases in the surface area of pigments prepared identically (assuming the porosity remains constant) should result correspondingly in an increase in solar absorptivity during UV exposure. It has also been observed that for pigments of equivalent particle morphology (size and surface area), UV caused solar absorptivity degradation was observed to increase with heat treatment temperature (calcination) of the pigment. Reaction rates of defect formation (related to impurity defects in the pigment) and therefore the solar absorptivity degradation, increase with higher temperature exposures. More degradation should result with higher temperature exposures resultant from pigment calcination.

IITRI hypothesized that the evolution of oxygen (oxygen desorption) from the pigment occurs during UV exposure resulting in optical property degradation. Bleaching of degraded pigments by oxygen has supported this theory.[14] A possible mechanism of optical property degradation may involve the irreversible loss of oxygen during high vacuum irradiation to the UV radiation. This degradation may be dependent on the oxygen diffusion rate through the pigment and binder. IITRI's research indicated that pigment purity, porosity, and crystalline perfection of the pigment material are typical properties that can influence the optical property stability of white thermal control coatings.

This methodology was employed by IITRI in the development of the S13G/L series of spacecraft thermal control coatings. From these studies it is evident that there is an optimum particle size distribution for maximum reflectance based on the particle sizes in the agglomerated particle and based on the refractive index of the compound. An agglomerated particle consists of colloidal-sized particles agglomerated into particles larger than 1 micron. In semiconductor type pigments such as titania (TiO_2, rutile) and zinc oxide (ZnO), the high extinction for UV radiation at wavelengths below their absorption edge (approximately 385 nm in zinc oxide) serves to effectively screen the UV radiation from the binder material. Dielectric pigments (e.g., Al_2O_3, MgO, SiO_2), are transparent to much of the solar UV radiation down to approximately 200 nm. These pigments effectively scatter UV radiation, which increases the possibility of spectral damage of the binder material. Another aspect of stability, regarding the preference of semiconductor over dielectric pigments, is the location of damage sites (or color centers). The UV transparency of the dielectric pigments such as Al_2O_3 or MgO suggests that the damage is related to bulk phenomena, with optical manifestations relating to, among other things, bulk diffusion processes (including the diffusion processes of the defects) of the crystal. Since damage occurs at relatively low temperatures, it is doubtful that diffusion processes are involved. Semiconductor pigments posses high extinction for damaging UV radiation and the damage is confined predominantly to the surface of the particles, where it can be treated more effectively. In UV irradiated zinc orthotitanate, an absorption band at 950 nm has been attributed to an electron trap associated with Ti^{+3} ions. Studies have shown that excess zinc oxide (0.5%), which leads to zinc oxide in solid solution with zinc orthotitanate, is essential in minimizing the production of Ti^{+3}. This absorption band is rapidly bleached with oxygen. Based on ESR studies, the

production of Ti^{+3} from UV irradiation is attributed to the photodesorption reaction of the general type previously shown in Equation 2. Heat treating the pigment increased UV stability, but proved more difficult to grind (to produce optimum particle size distribution for optimum reflectance) which is a major difficulty in manufacturing the pigment for this application. IITRI found that by encapsulating zinc orthotitanate particles with the potassium silicate binder that optical degradation was reduced.

In addition IITRI studies have emphasized the importance of performing the UV irradiation in a vacuum environment in order to replicate the degradation mechanisms experience in the space environment.[2] Simulation and exposure of space radiation environments are important characterization methods for determining the degradation mechanisms of thermal control coatings. Degradation mechanisms are influenced by defects and impurities in the coating and by the environment (or simulated environment) to which they are exposed. Knowing the manifestations of these effects, it is possible to better understand and characterize thermal control coatings for future applications.

2.3 Color Centers and Defect Classification

The term Color Centers applies to special electronic configurations in a solid that give rise to optical absorption in a normally transparent spectral region. Color centers have been the interest of researchers since their initial discovery. Different color centers can be distinguished by their optical absorption frequencies.

In 1937 deBoer proposed in alkali halides a model for "F" center as an electron trapped at the position of missing halogen atom (halogen ion

vacancy).[23] Seitz proposed specific model of other color centers in alkali halides involving electrons and e^- deficiencies (positive holes) trapped at aggregates of anion and cation vacancies.[23]

Color center formation mechanisms are associated with interactions between point defects and electronic defects (electrons and holes). The latter can be formed by radiation having an energy greater than the electronic band gap of the material. An electron is raised from the valence band to the conduction band leaving a hole in the valence band. The electrons are mobile in the conduction band and the holes are mobile in the valence band permitting reactions between these electronic defects and point defects. Point defects can be either substitutional or interstitial impurities as well as vacant lattice sites. The latter two are always present in normal crystals being required by the second and third laws of thermodynamics. The most characterized color center is the F center which is considered to be an electron combined or trapped at an anion vacancy as shown in Equation 4;

$$V_{anion}^{\bullet} + e' \Rightarrow (V_{anion}^{\bullet}, e')^{x} \qquad (4)$$

where the x denotes a neutral species. Visible coloration is observed as a result of the hydrogen atom-like electronic transitions of the trapped electron as it orbits the positively charged anion vacancy. Electron holes trapped at negatively charged cation vacancies and/or adjacent anions lead to a host of color centers more nearly in the UV region and are referred to as V centers.

Ionizing radiation can change the valence state of a point defect impurity leading to coloration. The coloration is induced by the optical absorption bands in the UV-visible spectrum associated with an altered impurity valence state. For example, the "solarization" or pink color developed in glass by UV radiation is caused by the (redox) reaction shown in Equation 5.

$$Fe^{+3} + Mn^{+2} \xrightarrow{h\nu} Fe^{+2} + Mn^{+3} \quad (5)$$

The coloration observed is due to the strong absorptions by electronic transitions in the Mn^{+3} ion. This coloration can be prevented by the addition of a strong reducing ion cerium, Ce^{+3}, so that the Mn ion is kept in the ($^{+2}$) state.

Oxide ceramics can be reduced in vacuum and reducing atmospheres to produce both electronic and lattice defects. These electronic defects can give rise to a spectrally broad absorption through free-carrier absorption.[24]

Defects in crystals can be caused by ionizing radiation, which is able to generate free electrons and holes (from ejected electrons) have been also been studied. Energy ranges reported to cause color center formation have been reported for ionizing radiation of 10 eV, for soft x-ray (10-60 keV), for gamma radiation of Co^{60} (1.25 MeV), and high energy protons of 100 MeV.[25] Ionization does not necessarily change stoichiometry of the crystal postulated, unless atoms are lost (ejected) from the surface of the lattice. Since a crystal must remain electrically neutral, it is an inherent characteristic of this type of coloration that both excess electron centers and excess holes centers are formed.

In alkali halides three common mechanisms have been postulated in generating lattice defects corresponding to color centers. The defect mechanisms, resulting from absorbed energy, in order of lowest to highest energy of formation, are; exciton formation, single ionizations, and multiple ionizations.[26]

An exciton is defined, for alkali halides, as an excitation of one of the valence electrons of a halogen ion to a bound excited state. When the ion relaxes to its ground state the same amount of energy as required to form the exciton will be released, usually in the form of luminescence[27]. The energy not

lost by luminescence will be transferred to the lattice. Experimental evidence has shown that this energy is not sufficient to produce simple color centers in pure alkali halide crystals.[27]

Single ionization is the removal of a halide valence electron from the ion resulting in a halide atom. This causes a relaxation around the halogen atom in the lattice. The halogen atom is now electrically neutral and is not electrostatically bound to the lattice site. The halogen atom is free to move, or diffuse, through the lattice creating an H center. The remaining vacancy could trap the ejected electron, resulting in an F center.[27]

In multiple ionization, both of the previously discussed mechanisms are involved. An incident photon interacts with the halogen ion in the crystal and doubly ionizes the halogen leaving a positive charged ion that will quickly trap an electron (due to its high electron affinity) resulting in a neutral halogen atom that is free to diffuse through the lattice, an H center. The resulting halide ion vacancy is left (in affect, a positive charge) to capture an electron and result in an F center.[28]

Another mechanism, proposed by Seitz, is the dislocation mechanism. Seitz postulated that dislocations are sources of vacancies that will in turn contribute to color centers or color center formation. Dislocations are generated from plastically deforming the crystal (from induced or inherent stresses) and then vacancies are formed during subsequent irradiation.[29] For plasma-sprayed coatings, in which the crystals are relatively unstrained this should not be of significant concern.

The influence of impurities upon coloration is quite marked. Ca^{2+} doped NaCl colors much more readily than pure NaCl. In this case the crystal behaves as if it contains a large concentration of negative ion vacancies that can be

easily freed by x-ray irradiation.[30] In contrast, Cd^{2+} doped NaCl that contained the same concentration of negative ion vacancies as Ca^{2+} doped NaCl, colors the same as the pure NaCl crystal.[31]

Mechanisms of conversion by irradiation of one of the types of color centers to another type are common throughout the literature. For example, intrinsic defects in a crystal when irradiated (with x-ray to visible radiation) will transform to a different color center that is verified using optical absorption. Subsequent heating of this newly generated color center may again transform it to another type of color center, along with the original color center, again verified by optical absorption.[32] Other types of defects can be a combination of any of the point defects discussed above.

Optical property characterization is the most common detection method of studying color centers. There is an abundance of literature on color centers studied by optical absorption in the region of 185 to 3000 μm.[33] Some studies have even observed this phenomenon at regions lower than 185 μm with UV instrumentation.[33]

The equilibrium of each point defect reaction is dependent on the others that results in multiple equations for defect concentrations, chemical activities and partial pressures, which makes solutions to solving, or understanding, overall problem very difficult. The techniques of qualitatively interpreting the simultaneous solutions to the overall point defect equations using Kröger-Vink (K-V) diagrams should be employed, or at least considered. K-V diagrams are log-log plots of defect concentrations versus oxygen pressure and are useful in determining the dominant defect as a function of pressure. An example of the generation of a K-V diagram for Fe_2O_3 is given to illustrate how defect concentrations vary with oxygen pressure at equilibrium and involving only

intrinsic vacancy (Shottky), intrinsic electronic, and nonstoichiometry defects. The point defect equations with their associated equilibrium constants are given in Equations 6, 7, and 8;

$$\mathbf{O} \Leftrightarrow 2V_{Fe}''' + 3V_O^{\bullet\bullet} \; ; K_S \tag{6}$$

$$\mathbf{O} \Leftrightarrow e' + h^{\bullet} \; ; K_i \tag{7}$$

$$O_O \Leftrightarrow \frac{1}{2} O_2 + V_O^{\bullet\bullet} + 2e' \; ; K_R \tag{8}$$

where **O** indicates a perfect crystal, and K_S , K_i , K_R are the equilibrium constants for Shottky defects, ionization, and nonstoichiometry, respectively. Simultaneously solving the three associated equilibrium equations with electroneutrality along with the four unknowns (concentrations of V_{Fe}'' , $V_O^{\bullet\bullet}$, e', $h^{\bullet}$) and plotting as a function of oxygen pressure results in the K-V diagram illustrated in Figure 3. Figure 3 illustrates the oxygen pressure dependency of the defect concentrations at equilibrium temperatures. This implies that the oxygen pressure environment at plasma spray temperatures or calcination temperatures can influence the dominant defect concentrations that could influence color center formation.

The concentration of the four defects and their oxygen pressure dependency in the different regions of Figure 3 are summarized in Table 6. The K-V diagrams are a very useful method, of graphic representation, showing what the defect concentrations will be at equilibrium temperatures.

Probably the most important criterion that must be considered when studying color centers is that pertaining to charge neutrality. The crystal must be electrical neutral at all times so the formation of a charged defect of one sign must be balanced by defects of the opposite sign.[34]

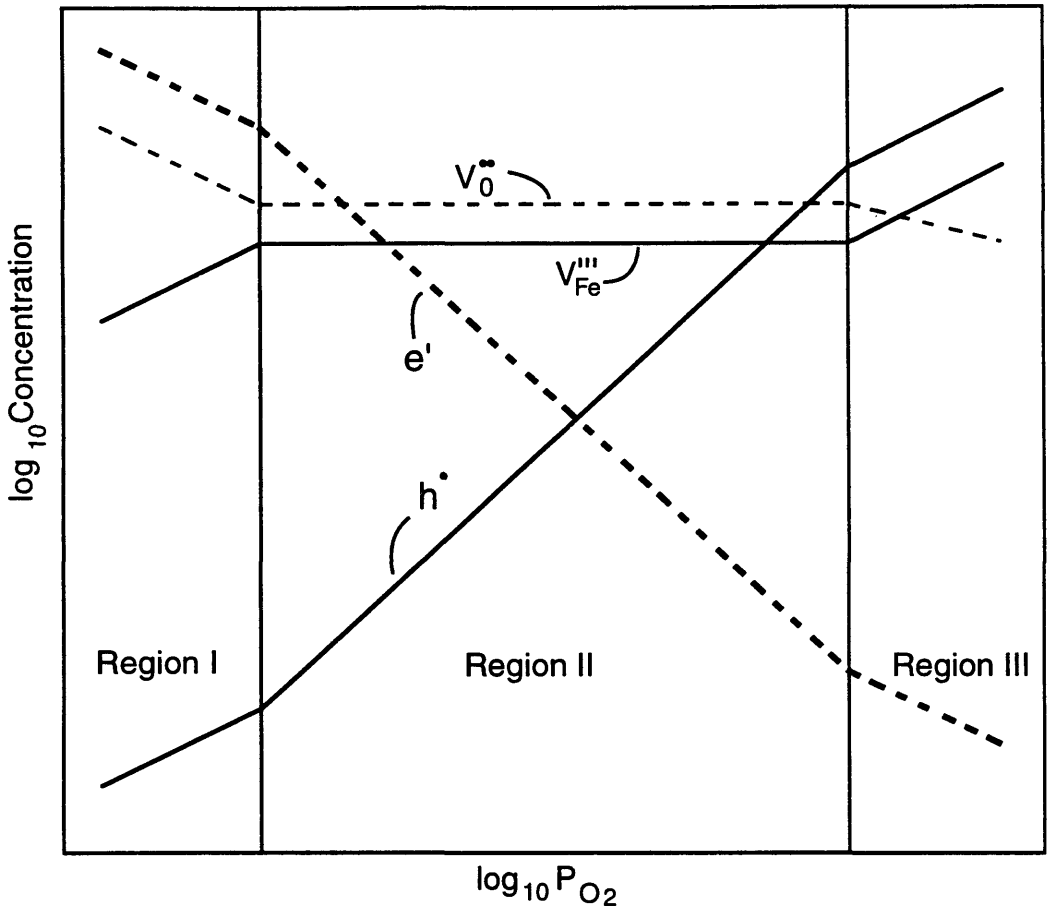

Figure 3 Kröger-Vink (K-V) Diagram for Fe_2O_3.

Table 6 Defect Concentration for the K-V Diagram (Figure 3).of Fe_2O_3

Defect Concentration	Proportional to $P_{O_2}^{exp}$		
	exp		
$h^{\bullet}$	1/6	1/4	3/16
e'	-1/6	-1/4	-3/16
$V_0^{\bullet\bullet}$	-1/6	—	-1/8
$V_{Fe}^{''}$	-1/4	—	3/16
	Region I	Region II Stoichiometric	Region III

3. EXPERIMENTAL

3.1 Overview

Economic considerations, optical property stability under radiation exposure, and optical property consistency led to the initial selection of the plasma-sprayed Ceramatec (Salt Lake City, Utah) BA200 sodium aluminate powder for continuation of development for thermal control coatings. The BA200 is a precursor powder developed to produce beta alumina (β-Al_2O_3). Plasma-sprayed coatings resulted in several unexpected advantages compared with current technology. From an environmental perspective, there are no organic solvents used in the cleaning or application process. Typical surface preparation involves cleaning the surfaces with aqueous cleaners and then blasting with an abrasive media, usually alumina grit. From a manufacturing viewpoint, the only real problem is applying this coating to surfaces of complex geometry. With proper planning and experience, this difficulty can be overcome. The resultant plasma-sprayed coating is extremely durable compared with other current coating technologies. The plasma-sprayed ceramic coatings withstand and resist abuse encountered in typical manufacturing operations. Usually when the plasma-sprayed coating is damaged, the optical properties can easily be restored by buffing the mar with a slight abrasive (i.e., pencil eraser). Organic contamination can usually be remove with isopropyl alcohol or acetone.

This research investigates and evaluates the plasma-spray optimization of the BA200 powder to achieve consistently low solar absorptivity. Simulated natural space environment testing was performed on selected samples to

characterize optical property degradation of the BA200 plasma-sprayed coatings. UV and e^- irradiation were performed independently (instead of the preferred combined environment testing) due to facility limitations. Doping of the BA200 powder with Ce_2O_3 (Ce^{+3}) to inhibit optical property degradation was performed and resultant plasma-sprayed coating was subjected to UV and e^- irradiation. Optical property characterization, limited physical property characterization, and simulated space environment exposures were performed on plasma-sprayed BA200 coatings to show their viability as spacecraft thermal control coatings.

3.2 Initial Screening

The initial screening of ceramic powders to be used for plasma-sprayed thermal control coatings was done prior to the work contained in this thesis. A literature search was performed on high temperature, white ceramic compounds and samples were obtained from various manufacturers. Plasma-sprayed coatings were produced with these ceramic powder samples. From this initial work the Ceramatec S4D BA200 powder was selected for further development because of consistent desirable optical properties.

Substrates used in this investigation were selected for low weight and high temperature capabilities. Molybdenum (Mo), Titanium (Ti), and Carbon-Carbon (C-C) substrates were selected. Optical properties of the resultant plasma-sprayed coatings initially investigated are given in Table 7.

From earlier studies[35], it was observed that plasma-spray parameters developed on Mo substrates resulted in different optical properties (higher solar absorptivity, α_s, values) when applied to C-C substrates. The increase in the α_s

Table 7 Optical Properties of Various Plasma-sprayed Coatings.

Powder (Manufacturer)	Substrate	α_s ave	ε_h ave	α_s min	α_s max
Al_2O_3					
OC-1000 hydrated (Alcoa)	Mo	0.25	0.86	-	-
calcined	Mo	0.28	0.83	0.23	0.33
105 SFP (Metco)	Mo	0.27	0.80	0.20	0.36
	C-C	0.44	0.80	0.25	0.57
	Ti	0.24	0.82	0.23	0.28
Linde C (Union Carbide)	Mo	0.33	0.80	0.26	0.46
PP-133 (Bay State)	Mo	0.44	0.63	0.37	0.53
PP-34 (Bay State)	Mo	0.29	0.80	0.26	0.30
PP-45 (Bay State)	Mo	0.29	0.84	-	-
Na_2O-Al_2O_3					
AlO-186 (Union Carbide)	Mo	0.24	0.87	0.22	0.28
	Ti	0.32	0.88	-	-
S4D BA200 (Ceramatec)	Al	0.26	0.89	0.20	0.29
	C-C	0.31	0.89	0.22	0.42
	Mo	0.27	0.89	0.17	0.45
ZrO_2/CaO					
805.1 (Stark)	Mo	0.56	0.81	-	-
ZrO_2/MgO					
(Stark)	Mo	0.31	0.81	-	-
ZrO_2/Y_2O_3					
204B-NS (Metco)	Mo	0.31	0.79	-	-
$ZrSiO_4$					
(GA Technologies)	Mo	0.28	0.87	0.20	0.31
(Cerac)	Mo	0.47	0.88	0.45	0.49
	C-C	0.48	0.88	0.45	0.52
(Dupont)	Mo	0.41	0.87	-	-

can be partially attributed to observations made while characterizing the plasma-sprayed coatings. It was shown that thicker alumina coatings (>15 mil) were significantly transparent (>10%) in the visible region where the α_s is heavily weighted. Other increases in the α_s values can be attributed to "non" optimized plasma spraying parameters on C-C substrates The substrate temperature and cooling rates (as well as the coating recrystallization rates) during the plasma spraying process can directly affect the α_s of the resultant coating Therefore an additional coating optimization effort was warranted to lower the α_s of resultant coatings.

3.3 Optimization of Plasma Spray Parameters

Optimization was performed with a Metco plasma-spraying system with the components listed in Table 1. The plasma gun is mounted on an AR2000[36] robot providing six degrees of freedom movement. Samples are mounted on an integrated turntable that allows movement for cylindrical parts.

Hydrogen and argon were used for the primary and secondary gases, respectively, for generating the plasma. The utilization of a mixture of gases is necessary to develop the proper thermal environment of the plasma that influences the melting of the ceramic powder particle. This mixture of gases ultimately determines the enthalpy of the plasma. The enthalpy of the plasma defines the thermal and velocity regimes to which the powdered ceramic particle is exposed to in order to partially liquefy the particle and accelerate it towards the substrate.

The plasma power is probably the single most important variable in the coating process. The plasma power is determined by the primary gas flow rate

and the plasma system amperage. When the plasma is initially ignited, a low flow rate of the primary gas is introduced into the plasma and resulting power of the plasma system can be calculated from the current and amperage used by the system. By increasing the primary (or secondary) gas flow rate, the amperage of the plasma system correspondingly increases, as well as the plasma power. Similarly, increasing the primary (or secondary) gas flow rate increases the plasma velocity and enthalpy. By optimizing and controlling the plasma enthalpy, repeatable plasma thermal and flow conditions can be established, thereby minimizing the influence of this variable on the resultant coating. By controlling the thermal environment to which the ceramic particle is exposed, defect introduction is controlled (either chemical or structural) which could affect the resultant coating's optical properties.

High purity nitrogen and air were used for cooling the substrate during the deposition process and to blow off coated samples (to remove residual powder).

For ease of understanding the variety of parameters that directly affect the α_s of plasma-spray coatings, the known process variables (both controllable and uncontrollable) are given in Table 8. The interrelationships of these variables are not well defined and are the emphasis of the coating optimization efforts. These variables can directly affect the recrystallization of the powder materials as the coating is formed. By adjusting variables (the controllable variables listed in Table 8), different physical properties of the crystalline structure are modified, which influence the α_s. The effects of the controlled variables listed in Table 8 on the α_S were not completely understood which warranted this investigation.

Table 8 Plasma-Spray Process Variables

Controlled Variables
Power and Plasma Conditions Current Voltage Amperage
Spraying Distance Between Gun and Substrate
Powder Feed Rate into Plasma
Cooling Nozzle Distance From Substrate
Gases Primary Gas Pressure and Flow Rates Primary Gas (Hydrogen) Purity Secondary Gas Pressure and Flow Rates Secondary Gas (Argon) Purity Cooling Gas Pressure and Flow Rates Powder Feeder Pressure and Flow Rates Powder Feeder Gas Purity
Plasma Gun Electrodes
Cooling Water Temperature At Chiller At Electrodes
Substrate Cooling Conditions, Type of Cooling Heat Sink Vacuum Fixture
Spray Traverse Speed, Linear feet per unit time

Uncontrolled Variables
Powder Chemical Purity and Particle Size Distribution
Substrate Cooling Conditions Back Surface Temperature Front Surface Temperature
Ambient Temperature Humidity Conditions During Spraying
Cooling Air Purity and Moisture Content

Optical properties of the resultant coatings were measured to correlate the effects of the variable of interest. X-ray diffraction of raw BA200 powder and resultant coatings was performed to establish the phases present in the coating.

A classical approach for optimization was performed where variables were changed independently each other, then the individually optimized parameter was maintained for a given coating thickness when evaluating other variables.

The gases used for developing plasma-sprayed coatings were air, argon, hydrogen, and nitrogen. Hydrogen and argon were investigated as the primary and secondary gases, respectively, used to generate the plasma. Both of these gases were procured as high purity welding gases. Air and nitrogen were for the cooling gases as required. High purity gases are utilized to minimize the introduction of contamination into the resultant coating that could have deleterious affects on the resultant ceramic chemistry and structure due to the high operating temperature of the plasma to which the powders are exposed.

3.4 Characterization

Solar absorptivity and thermal emissivity measurements were measured on each coating sample. In addition the thickness of each sample was measured using a micrometer. UV-visible reflectance, x-ray diffraction, and infra red reflectance spectra were generated on selected samples. These data were used to assist in the optimization of the plasma-spray parameters during the experimentation. A brief description of each of the characterization methods and instrumentation used is contained in the following sections.

3.4.1 Solar Absorptance

A Gier-Dunkel Model MS251 Solar Reflectometer was used to provide quick measurements of α_s. This measurement was performed on all samples.

UV-visible reflectance spectra were generated on selected samples from which the solar absorptivity (α_s) was determined by integrating spectral hemispherical reflectance measurements over the solar spectrum, 0.25 μm to 2.5 μm. A weighting factor for specified spectral regions was used to calculate α_s. The weighting factor and corresponding wavelength ranges used in performing this calculation are given in Table 9. UV-visible reflectance spectra were generated on a Beckman Model DK-2A Ratio Recording Spectrophotometer.

Table 9 UV-Visible Spectral Reflectance Weighting Factors.

Wavelength Range (μm)	Factor		Wavelength Range (μm)	Factor
2.370 - 2.500	0.04		0.660 - 0.750	0.1
2.000 - 2.370	0.02		0.590 - 0.660	0.1
1.800 - 2.000	0.02		0.520 - 0.590	0.1
1.640 - 1.800	0.02		0.450 - 0.520	0.1
1.510 - 1.640	0.02		0.400 - 0.450	0.07
1.330 - 1.510	0.04		0.350 - 0.400	0.03
1.210 - 1.330	0.04		0.342 - 0.350	0.02
1.100 - 1.210	0.04		0.315 - 0.342	0.02
0.900 - 1.100	0.1		0.295 - 0.315	0.01
0.750 - 0.900	0.1		0.230 - 0.295	0.01

3.4.2 Emittance and Spectral IR Reflectance

Room temperature total normal emissivity (ε_n) were determined on all samples with a Gier-Dunkel Infrared Reflectometer Model DB100 that determines ε_n from 5 μm to 25 μm. Spectral hemispherical reflectance was determined on select samples from 2 μm to 25 μm with a Mattson Polaris Fourier Transform Infrared (FTIR) Spectrophotometer.

3.4.3 Ceria Doping of the BA200 Powder

Doping of the BA200 powder with Ce_2O_3 (Ce^{+3}) to inhibit optical property degradation was performed and the resultant plasma-sprayed coating was subjected to UV and e^- irradiation. Samples BA200-A and BA200-B were prepared using BA200 powder that was doped with 0.1% Ce_2O_3. After doping the powder was calcined (in an alumina crucible) in an air furnace at 1000°C for 24 hours. Samples BA200-A and BA200-B were plasma-spray coated from the doped powder.

3.4.4 Ultraviolet and Electron-Beam Test Exposure

An ultraviolet (UV) exposure chamber was used to provide evaluation of thermal control coatings from solar UV radiation (130 to 475 nm) exposure. A schematic of the environmental exposure chamber is shown in Figure 4. The samples were irradiated in the sample plane of the chamber, and a transport rod was used to position each sample in the integrating sphere for in-situ solar absorptivity measurements using a DK-2A spectrometer (0.25 μm to 2.5 μm).

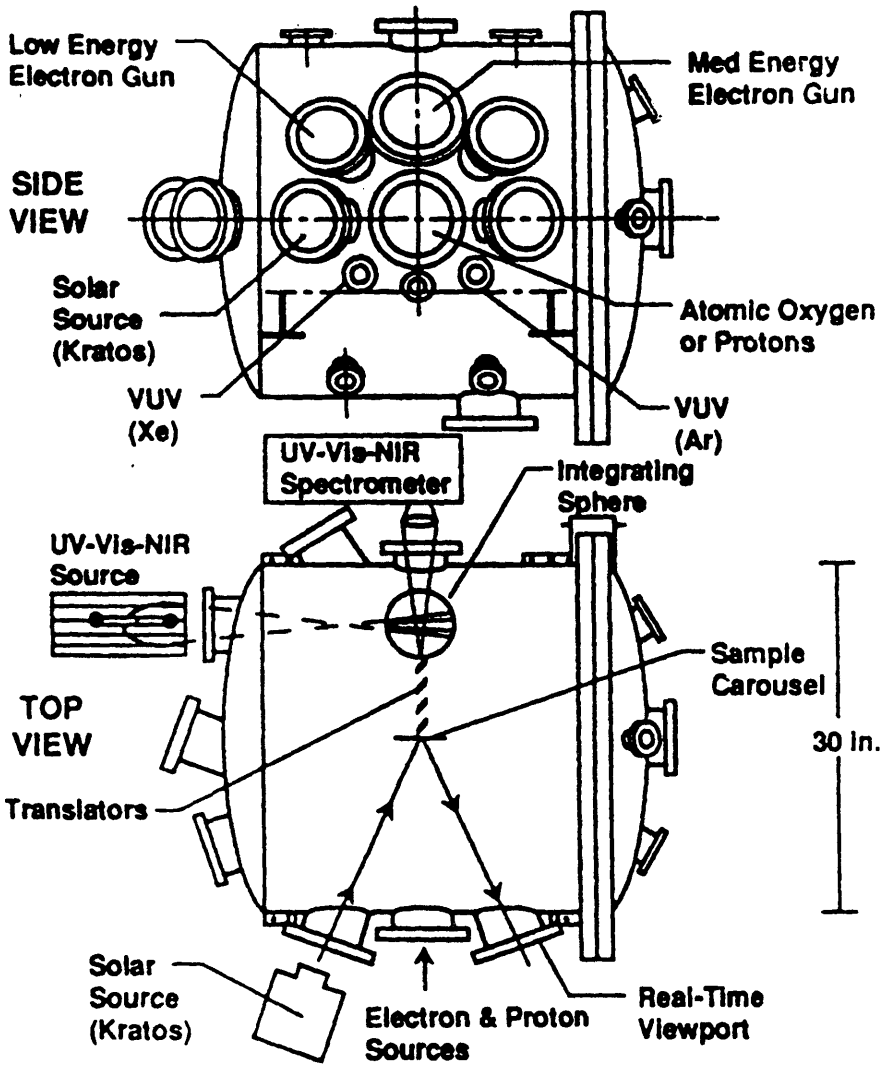

Figure 4 Space Environments Test Chamber

An 8-inch cryopump provided an oil-free vacuum environment in the low 10^{-6} torr range. The samples were irradiated for 1000 equivalent UV sun hours (EUVSH). A comparison of the simulated spectral energy distribution to the actual solar UV spectrum is shown in Figure 5. The irradiance of the UV source was set at 236 W/m^2 which corresponds to 2 equivalent UV (EUV) suns. The UV source was calibrated before and after exposure with a National Institute of Standards and Technology (NIST) calibrated photo-diode.

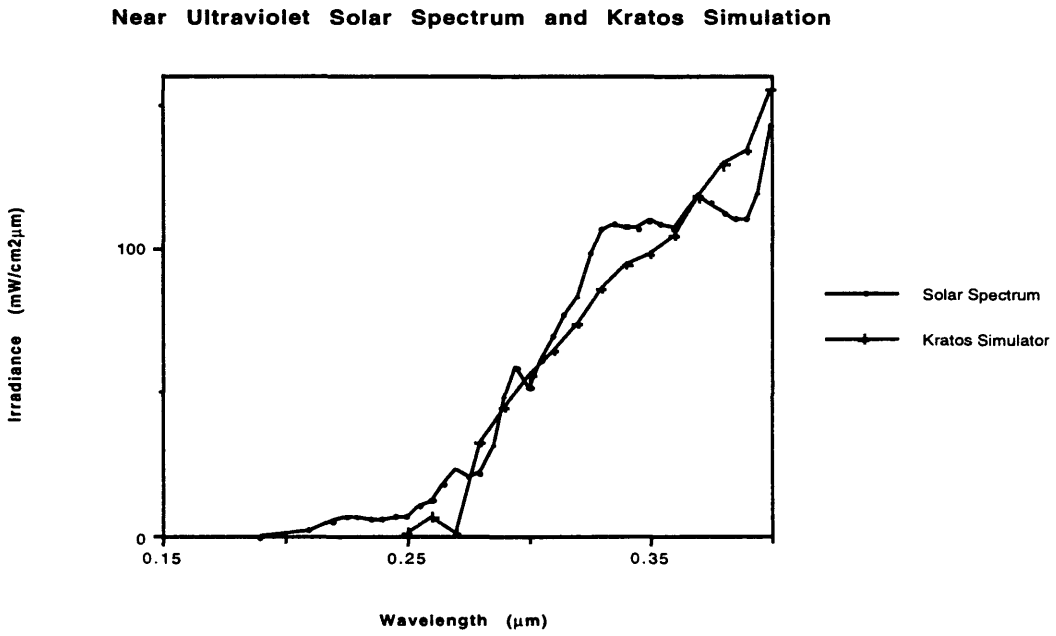

Figure 5 UV Solar Spectrum and Kratos Simulation Spectrum

An electron-beam exposure chamber was used to provide evaluation of thermal control coatings from low-energy (3 to 12 keV) electron exposure. The schematic of the environmental exposure chamber is shown in Figure 4. The samples were irradiated in the sample plane of the chamber, and a transport rod was used to position each sample in the integrating sphere for in-situ solar absorptivity measurements with the DK-2A spectrometer (0.25 μm to 2.5 μm). An 8-inch cryopump provided an oil-free vacuum environment in the low 10^{-6} torr range. A Faraday cup was positioned on the sample holder to monitor the flux from the electron gun mounted on the e^- beam port. The samples were irradiated with an electron fluence equal to a 5-year spacecraft mission with a flux of 10^9 $e^-/cm^2 \cdot sec$ over for 500 hours.

In-situ measurements were preferred since white thermal control materials can experience bleaching or annealing effects as a function of ambient environment exposure.

3.4.5 X-ray Diffraction

Crystalline structure determinations were performed on select samples with a Rigaku X-ray Diffractometer system with a Rotoflex RU-200 12-kW copper rotating anode.

3.4.6 Coating Thickness

Thickness measurements were measured on all samples with a micrometer. These data were used to assure thicknesses between individual coating samples were consistent when comparing each spray parameter optimization step.

ARTHUR LAKES LIBRARY
COLORADO SCHOOL OF MINES
GOLDEN, CO 80401

3.4.7 Effect Heat Treatments on Optical Properties

A decrease in the solar absorptivity of BA200 coatings had been previously observed after exposure to extreme temperature.[35] To further investigate this phenomenon, three BA200 coated samples were exposed to ~1200°C for ~30 minutes and two samples were exposed to ~1200°C for ~5 minutes while contained in an alumina crucible. Thermal exposure was performed at less than 10^{-6} torr pressure.

4. RESULTS

4.1 Plasma Spraying Parameter Optimization

The optimization of BA200 coatings was focused on varying the plasma-spray parameters shown in Table 10. Variables shown in Table 11 were not changed during the optimization investigation. The uncontrolled variables previously discussed were kept as constant as possible. All coatings were produced from a single lot of the BA200 powder. All gases used were of constant purity required by procurement specifications. Thickness and optical properties were measured on all coating samples produced.

Table 10 Plasma-Spray Optimization Variables

Optimized Variables	High	Low
Plasma Power (kW)	42	35
Powder Feed Rate into Plasma (g/min)	33	4
Spray Cycles	16	4

Table 11 Plasma-Spray Constant Variables

Constant Variable	Value
Spraying Distance (inches)	3.5
Spray Traverse Speed (mm/sec)	800
Cooling Nozzle Distance From Substrate (inches)	4
Substrate Cooling Conditions	Heat Sink
Cooling Water Temperature At Chiller (ºF)	68

A summarized graphical presentation of the effects of various plasma-spraying parameters previously generated with the S4D BA200 powder follows to illustrate the relationships (or interrelationships) upon how varying these parameters effects the solar absorptivity (α_s). The range of α_s and frequency or number of samples with that value of α_s produced during this investigation for molybdenum and C-C substrates are shown in Figure 6 and Figure 7 respectively. Zero frequency values means no samples were measured with that particular α_s. These figures represent all the samples prepared in this investigation and are intended to show the range of α_s resulting from the plasma-spray coating process. Understandably, this is the reason why process optimization to produce consistent coatings was needed.

Initial studies surrounding the plasma power setting have indicated that the optimal power setting for the BA200 powder is greater than 35 kW and in the range of 37.5 to 42 kW. The traverse speed observed in the initial studies was 800 mm\sec. Since a classical approach (examining each parameter independently of the others) was chosen to investigate the plasma-spray variables, the traverse speed of 800 mm/sec was chosen to remain constant throughout this investigation.

For the optimization, BA200 coatings were produced with the power settings of 35, 37.5 and 42 kW, keeping other variables constant. Figure 8 shows plasma power plotted against α_s obtained on molybdenum substrates. C-C substrates were sprayed predominantly at 37.5 kW with two samples sprayed at 35kW. These data for C-C are shown in Figure 9. The data at 35 kW were for larger surface area samples. Review of these data, with thickness considerations in mind, indicates that 37.5kW produced the lowest solar absorptivity.

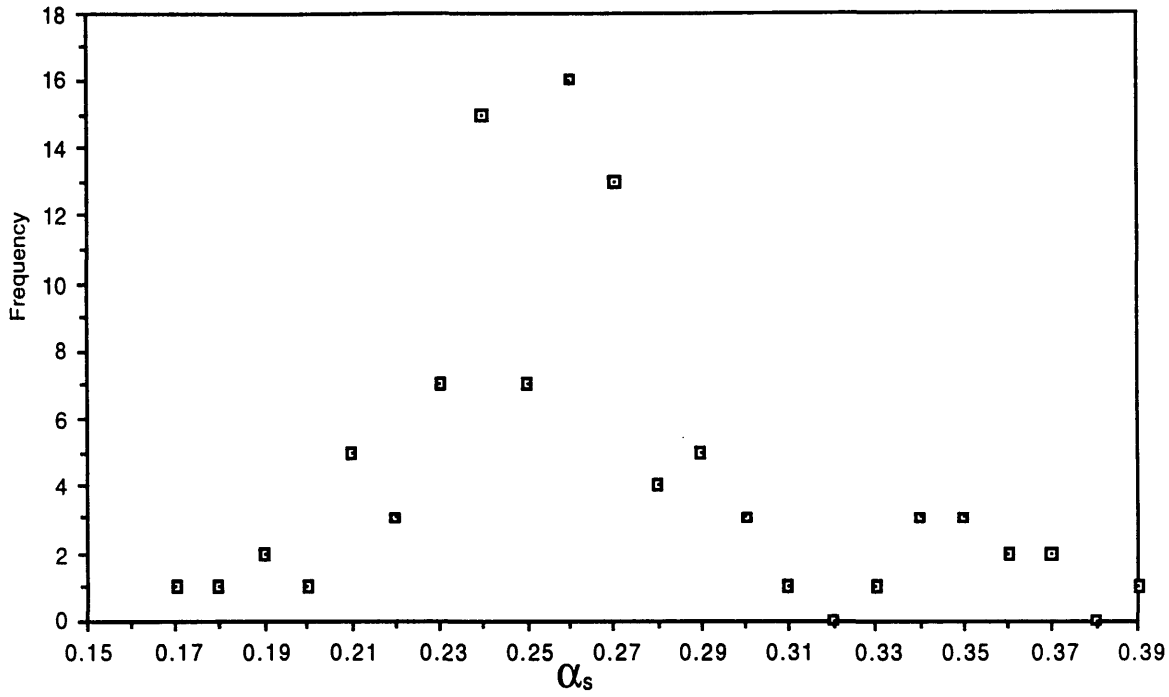

Figure 6 Distribution of α_s for BA200 on Mo

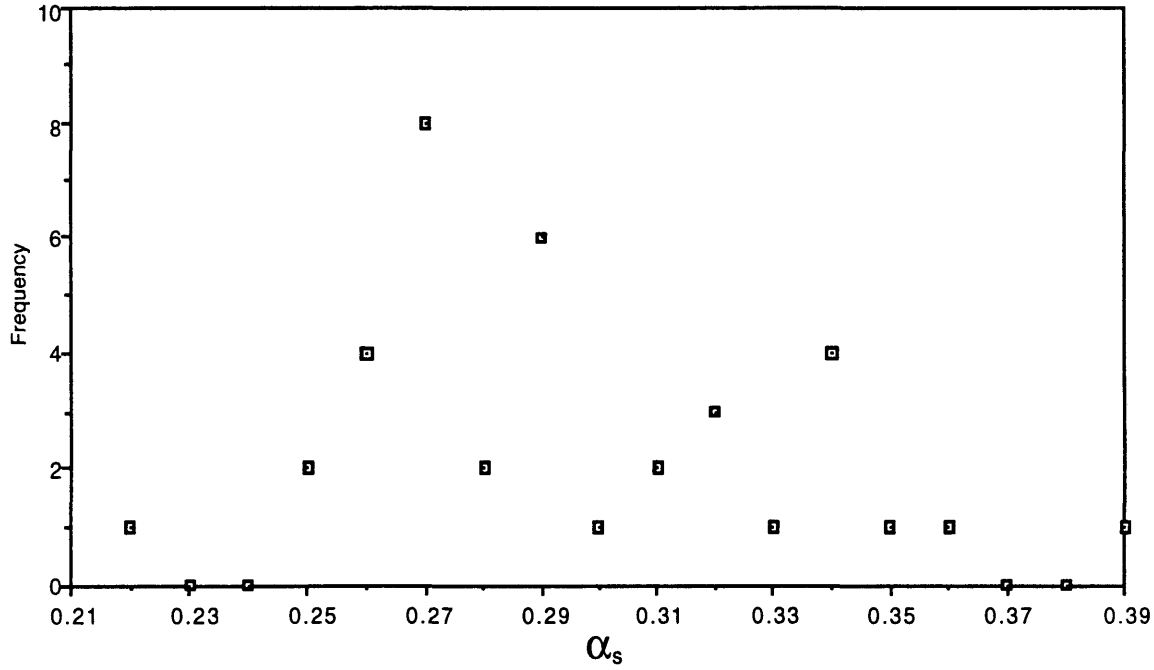

Figure 7 Distribution of α_s for BA200 on C-C

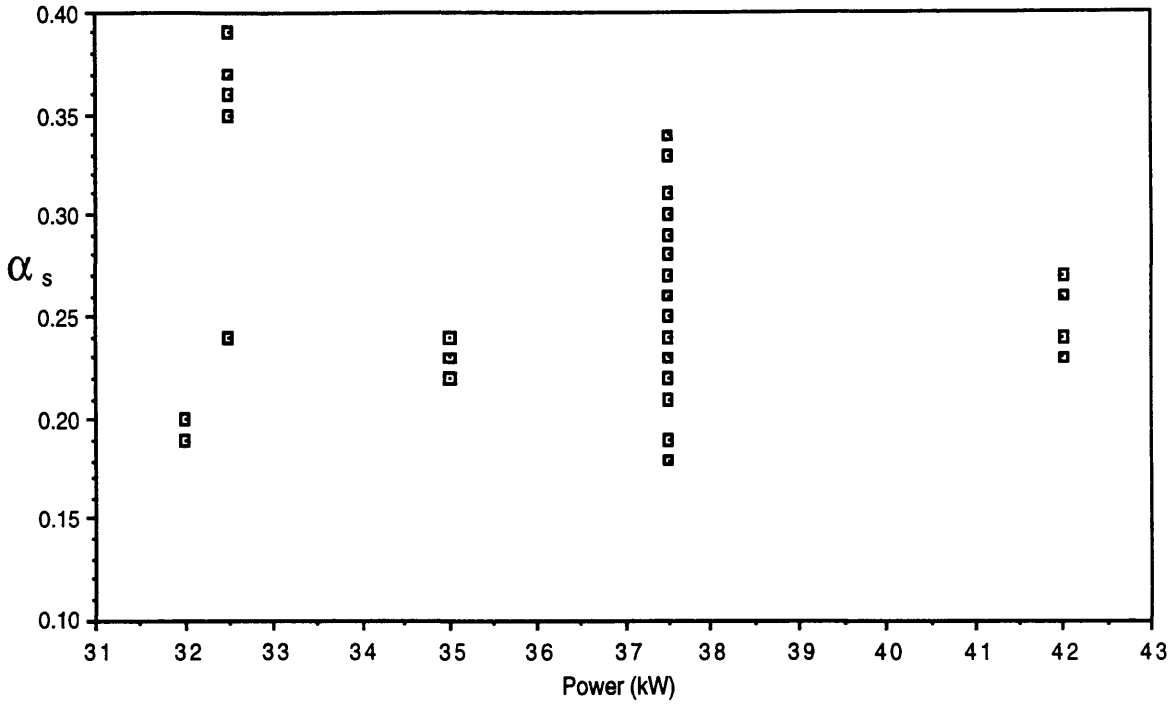

Figure 8 Power Setting Influence on α_s for BA200 on Mo

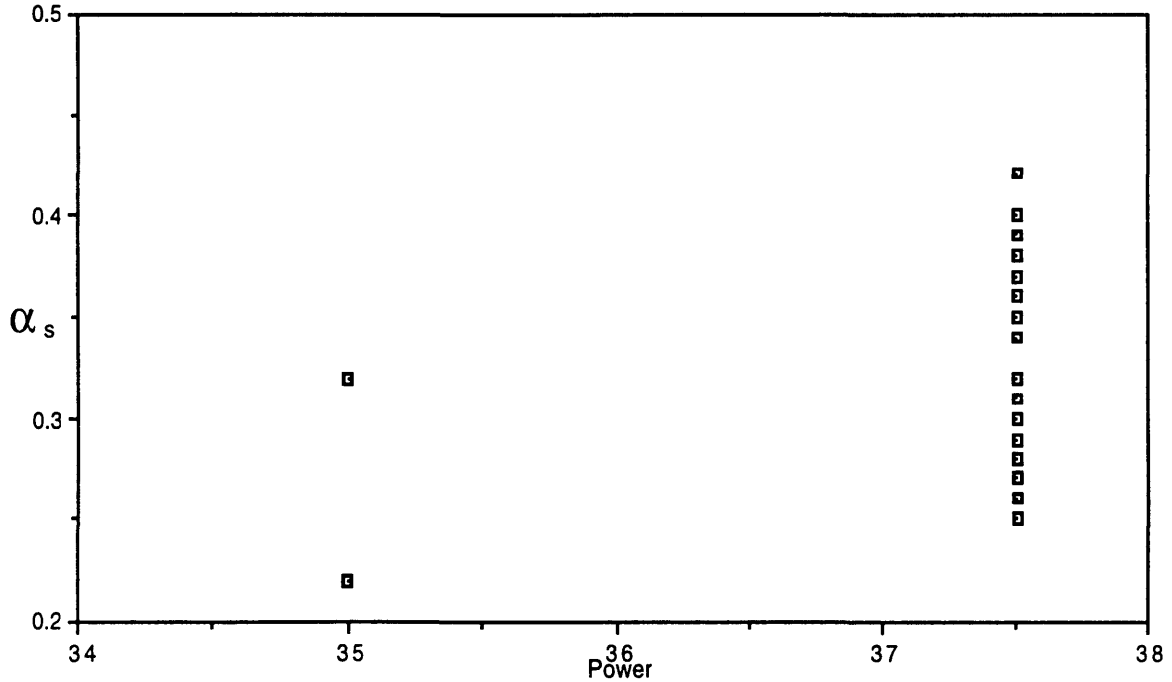

Figure 9 Power Setting Influence on α_s for BA200 on C-C

With a power setting at 37.5kW and traverse speed of 800 mm/sec, samples were generated varying the number of spray cycles (spray passes) and the powder feed rate (the rate that the powder is injected into the plasma). These data were then combined and the α_s was plotted against thickness on Mo, thickness on C-C, cycles on Mo, mils / cycle on Mo, and powder feed rate on Mo. These data are shown in Figure 10, Figure 11, Figure 12, Figure 13, and Figure 14 respectively.

The thickness of the BA200 coating was not controlled, but interesting correlation with lower α_s is seen in Figure 10 and Figure 11. From these figures it is apparent that coating thickness most important variable influencing the α_s.

4.2 Optical Property Characterization of BA200 Coatings

UV-visible spectral reflectance measurements were performed on pre-optimized and post-optimized BA200 coatings. These spectra are shown in Figure 15 .

Infrared spectral reflectance measurements were performed on pre and post optimized BA200 coatings. These spectra are shown in Figure 16 and Figure 17 respectively.

4.3 X-Ray Diffraction (XRD) of BA200 Coatings

X-ray diffraction (XRD) was performed on three coatings and on the raw BA200 powder as shown in Table 12. XRD spectra for these samples are shown in Figure 18, Figure 19, Figure 20, and Figure 21 as indicated in Table 12.

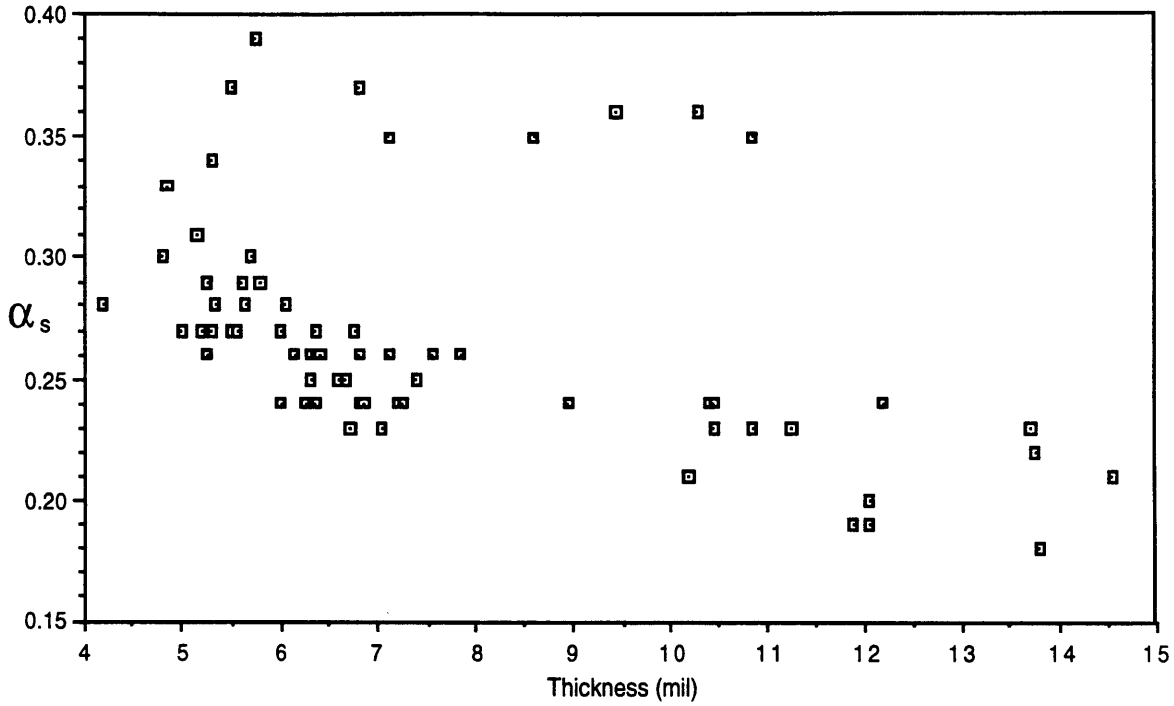

Figure 10 Thickness Influence on α_s for BA200 on Mo

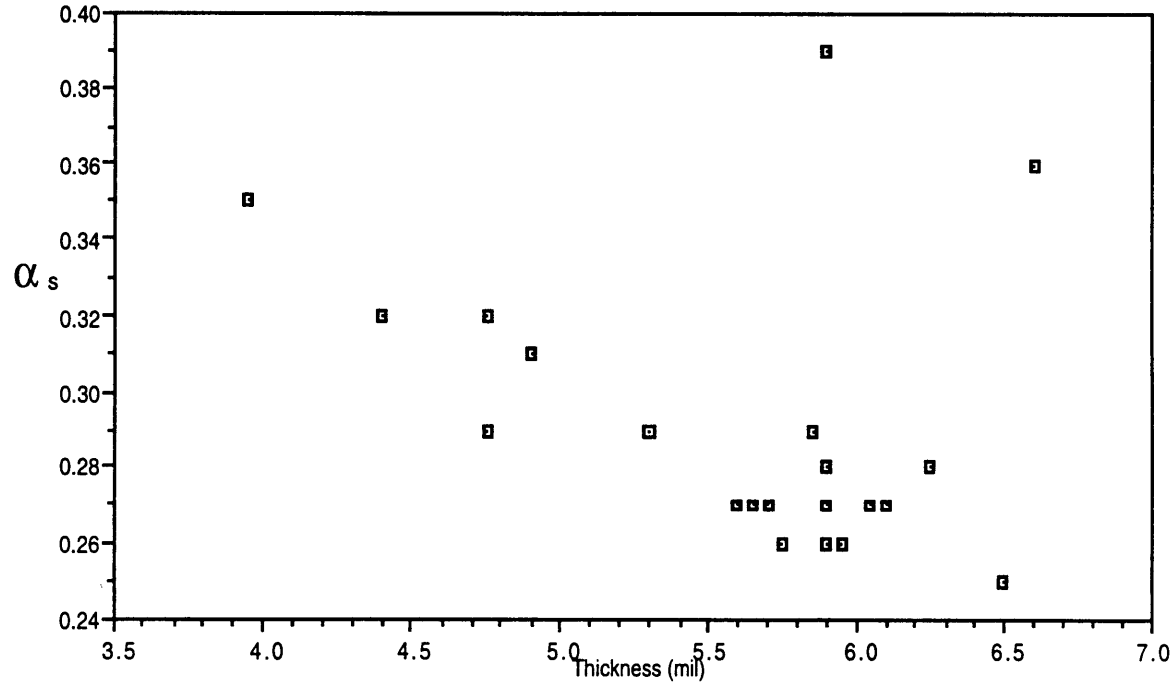

Figure 11 Thickness Influence on α_s for BA200 on C-C

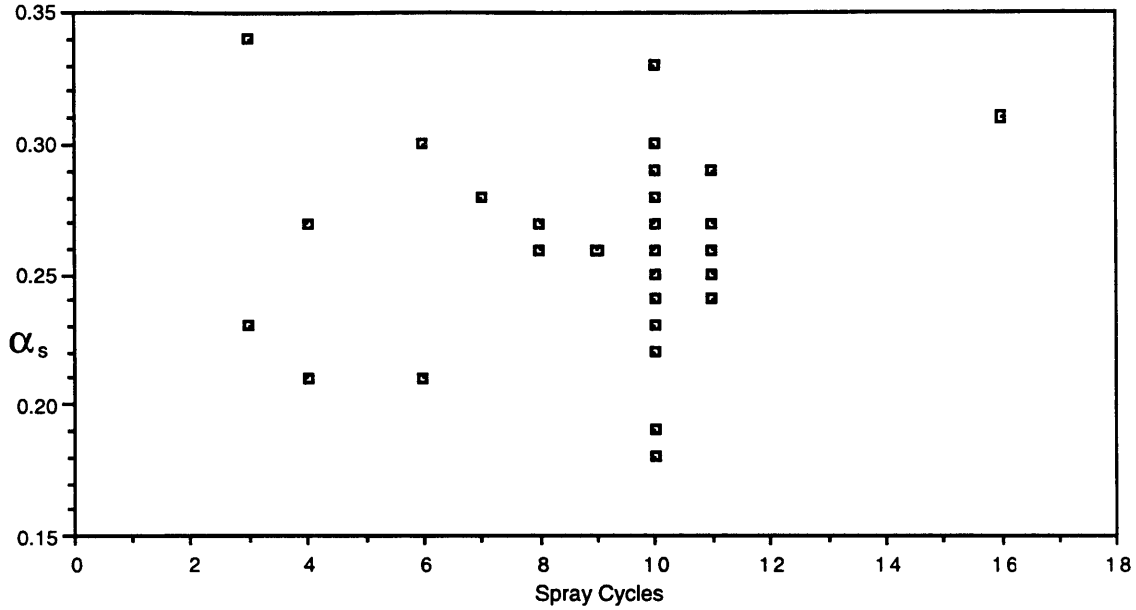

Figure 12 Spray Cycle Influence of α_s for BA200 on Mo

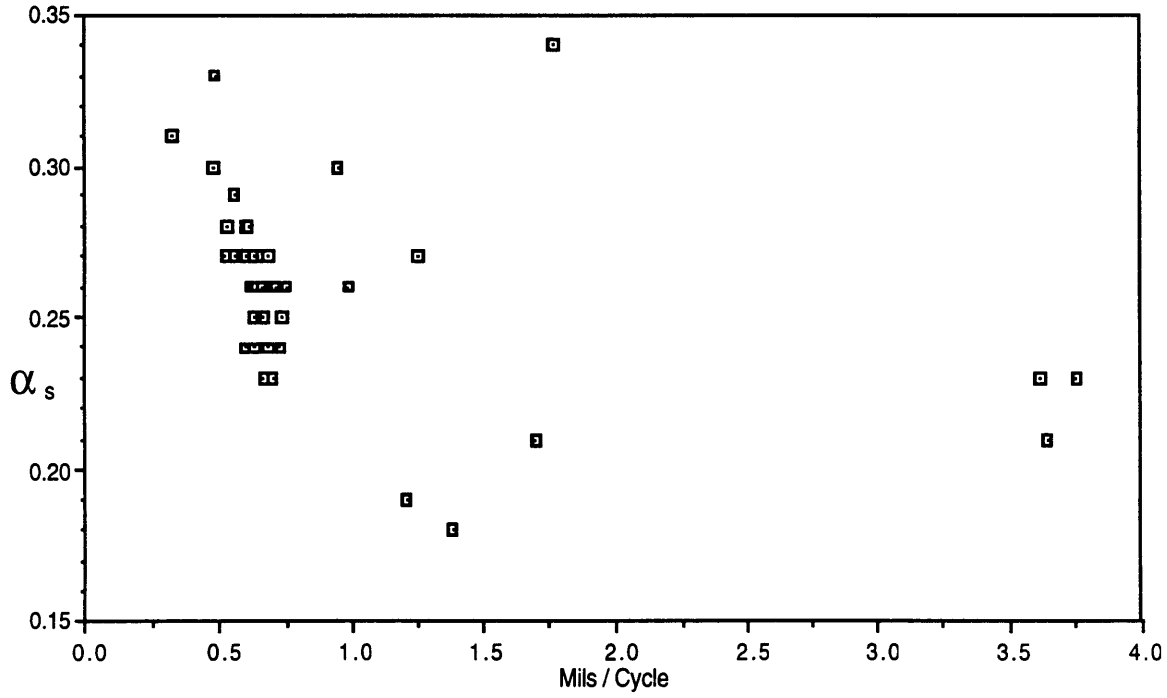

Figure 13 Mils Coating / Spray Cycle Influence on α_s for BA200 on Mo

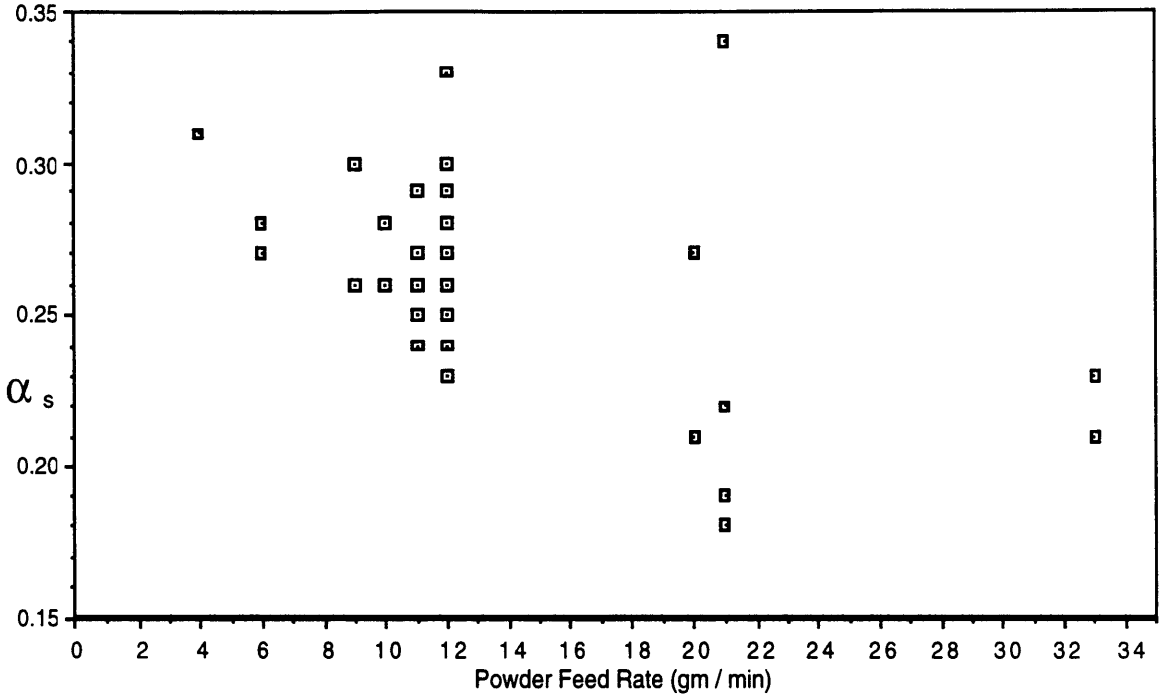

Figure 14 Powder Feed Rate Influence on α_s for BA200 on Mo

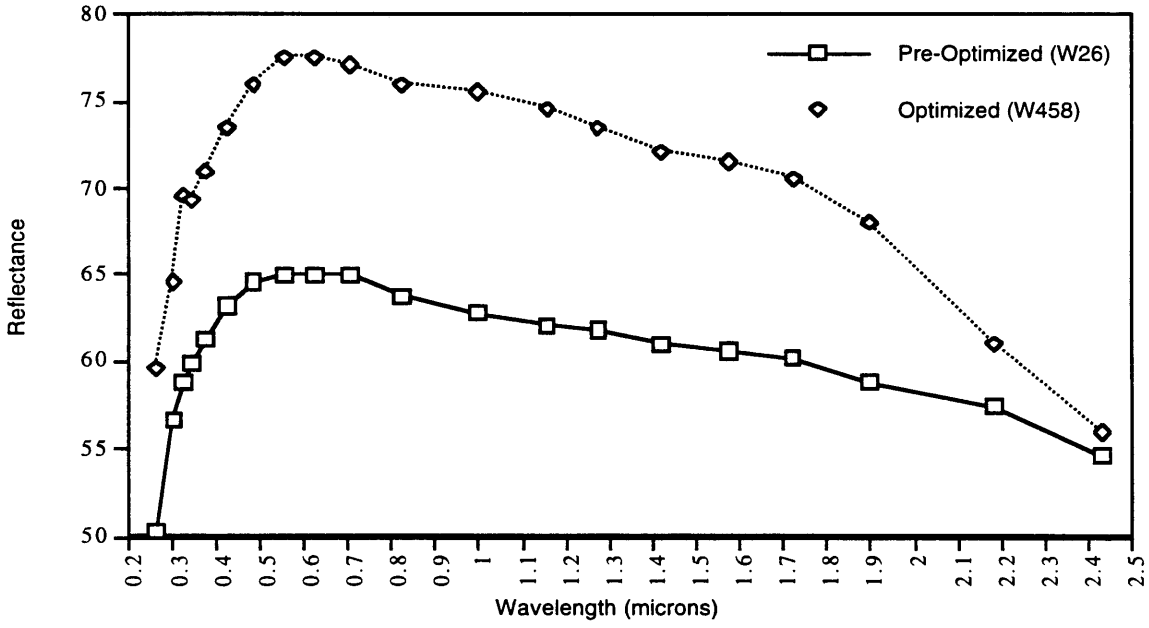

Figure 15 Pre and Post Optimization UV-Visible Reflectance

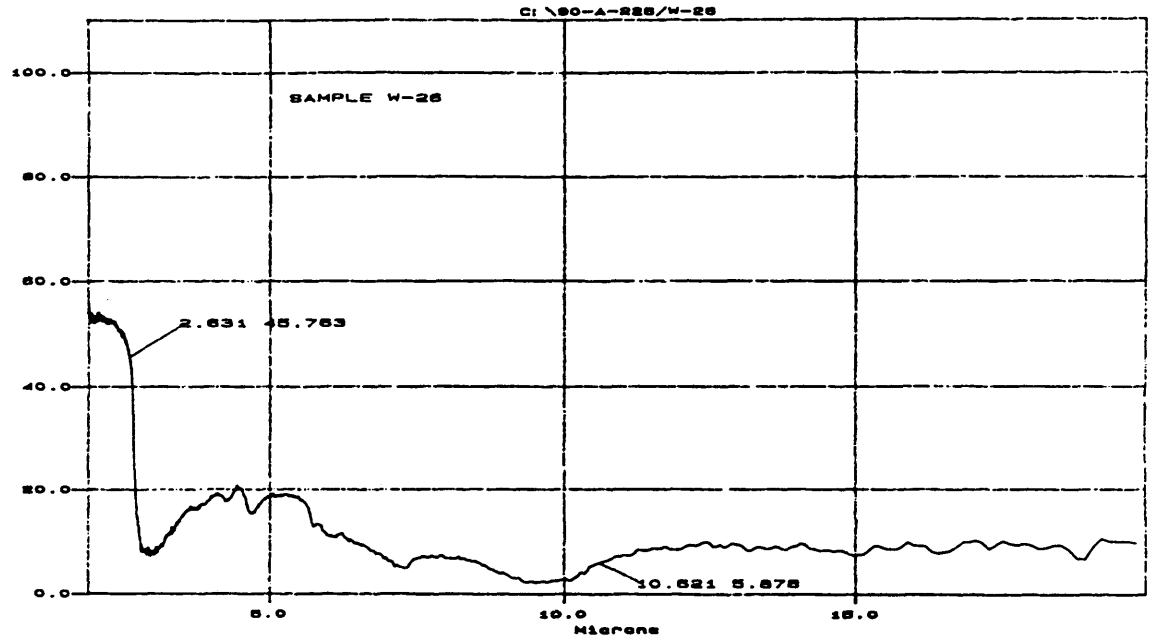

Figure 16 Pre Optimization Infrared Reflectance Spectra

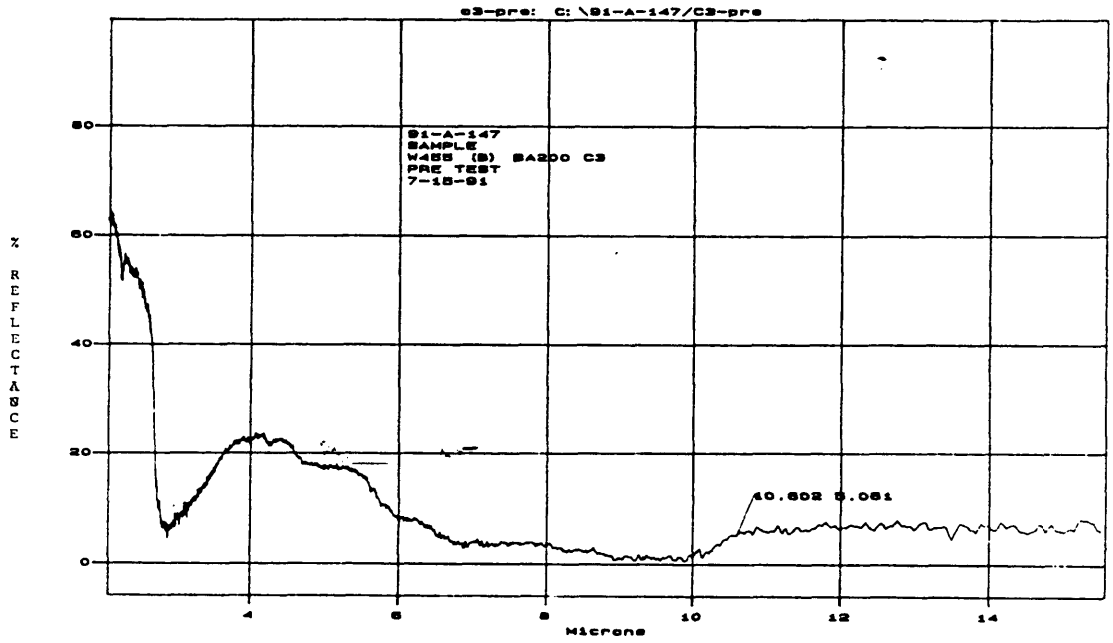

Figure 17 Post Optimization Infrared Reflectance Spectra

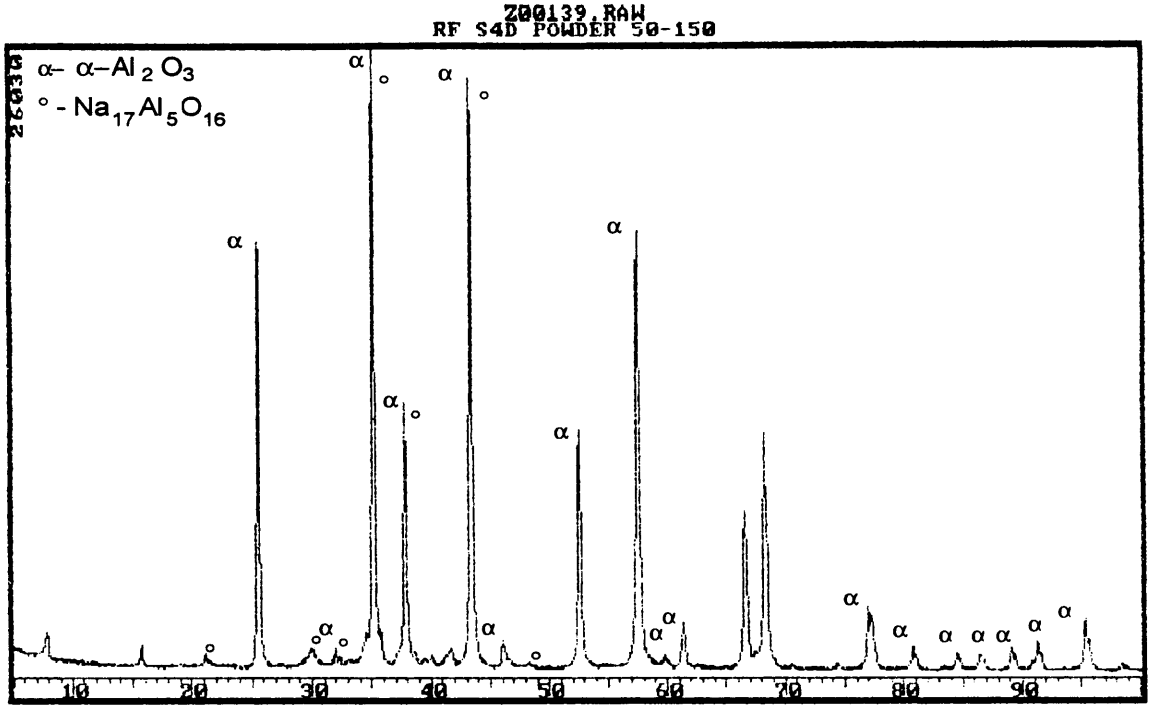

Figure 18 XRD Spectrum of BA200 Powder

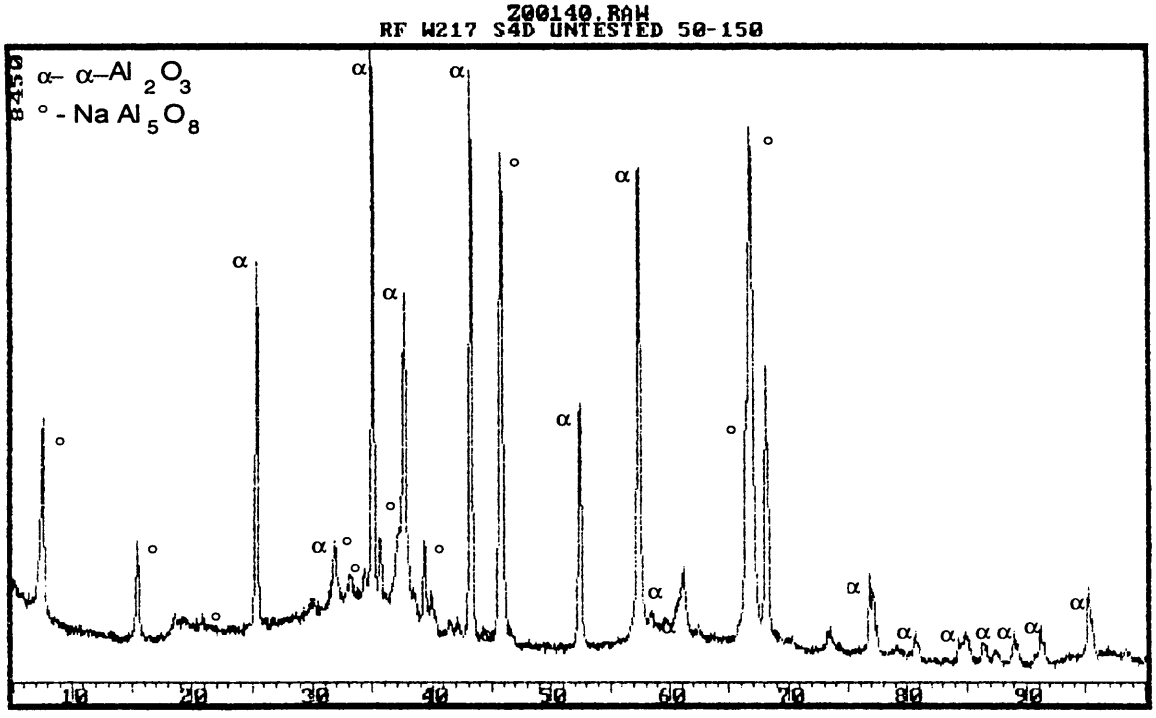

Figure 19 XRD Spectrum of Unoptimized BA200 Coating

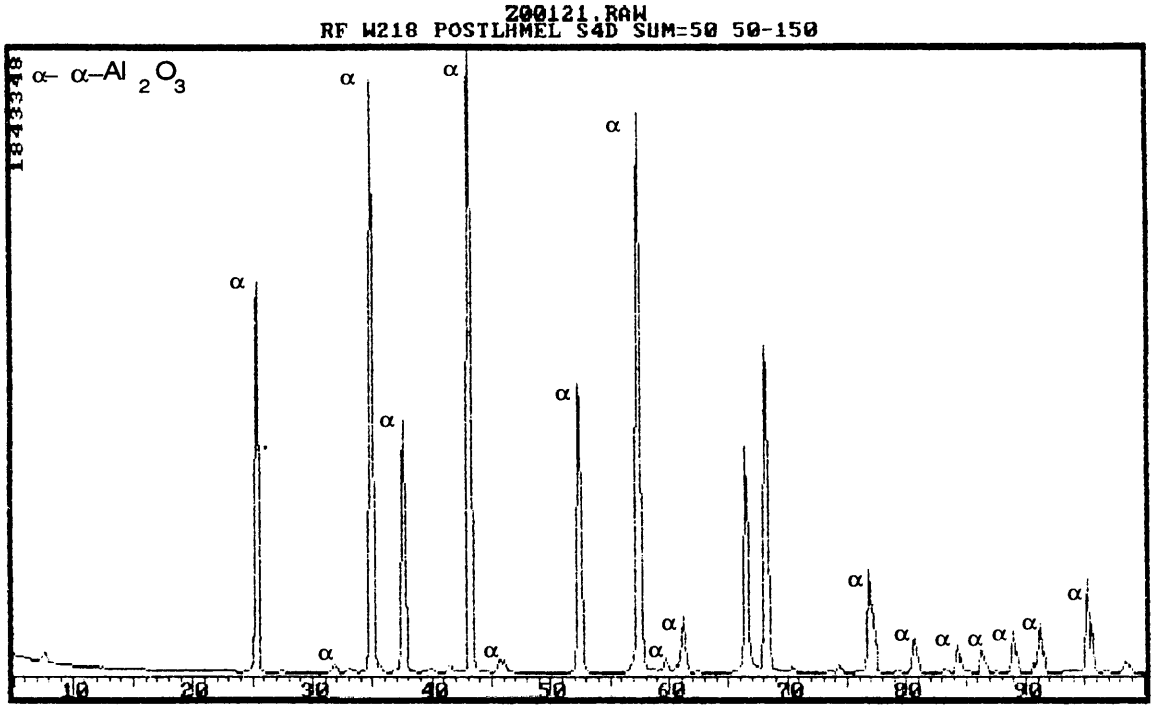

Figure 20 XRD Spectrum of Heat Treated Unoptimized BA200 Coating

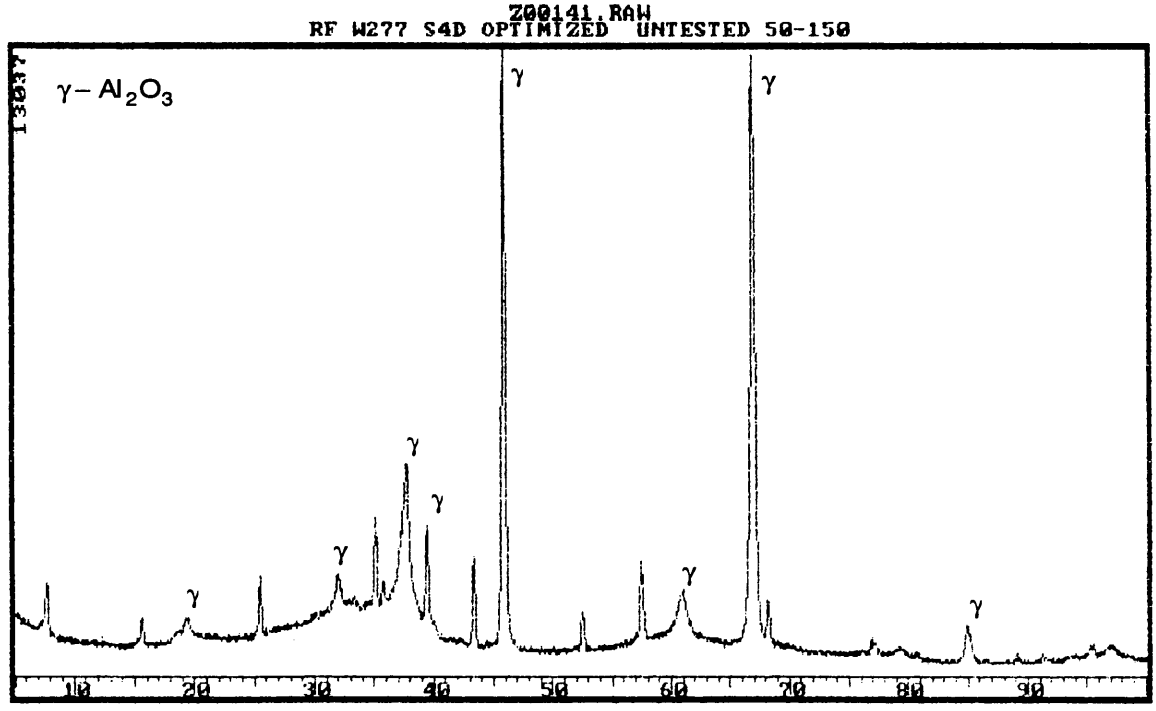

Figure 21 XRD Spectrum of Optimized BA200 Coating

Table 12 XRD Samples

Description	Solar Absorptivity (α_s)	Figure Reference
A - BA200 Powder, as received	-	Figure 18
B - Unoptimized Coating	0.35	Figure 19
C - Unoptimized Coating Exposed to ~1200C for ~ 3 minutes	0.13	Figure 20
D - Optimized Coating	0.18	Figure 21

Identification of these spectra with a computer JCPDS file matching program revealed that the BA200 coatings were predominantly crystalline α-Al_2O_3. (JCPDS file 10-173). The raw BA200 powder was predominately α-Al_2O_3 and showed evidence of a sodium aluminum oxide compound (JCPDS file 38-36, $Na_{17}Al_5O_{16}$). The manufacturer of this powder confirmed that the BA200 was supplied as a mixture of α-Al_2O_3, sodium hydroxide, and lithium hydroxide.

The unoptimized BA200 coating again showed predominately α-Al_2O_3, with possible matching to a sodium aluminum oxide compound (JCPDS file 19-1173, $NaAl_5O_8$). The heat treated unoptimized BA200 coating again showed predominately α-Al_2O_3. The optimized BA200 coating indicated that γ-Al_2O_3 (JCPDS file 10-425) was predominate.

4.4 Effects of Heat Treatment

Optical property changes of S4D BA200 coatings after severe thermal exposure have been consistently observed. Experiments were performed to try to replicate the temperatures measured during previous thermal exposure, and then observe any optical property changes. Three tests were conducted and their results are described in the following section. Optical property data and observations for these tests are given in Table 13.

4.4.1 Heat Treatment Test 1

Two BA200 coated samples (HT-1 and HT-2) were placed in a vacuum furnace (without precleaning of the coated side or backside) and exposed to ~1200°C for ~30 minutes. Both of these samples were severely discolored gray during this heat treatment. A alumina coating sample (plasma-sprayed using Metco 105SFP powder) was also heated concurrently with the BA200 samples with no visible discoloration. The BA200 sample, HT-1, was then submitted for Auger, secondary ion mass spectroscopy (SIMS), and energy dispersive x-ray spectroscopy (EDX) analyses. The Auger, SIMS and EDX spectra, shown in Figure 22, Figure 23, and Figure 24, respectively. All spectra show conclusively the presence of chromium (Cr). EDX spectra additionally showed the presence of iron (Fe).

Table 13 Results of Bake-Out of BA200 Coatings on Mo Substrates

		Pre		Post		
Sample ID	Test	(α_s)	(ε_{RT})	(α_s)	(ε_{RT})	NOTE
HT-1	1			-	-	(A) severe gray discoloration
HT-2	1			-	-	(A) severe gray discoloration
HT-3	2			-	-	Yellowish discoloration
HT-4	3	~0.25	~0.90	0.26	0.85	
HT-5	3	0.24	0.90	0.18	0.87	whitened considerably

Test 1 ~1200°C for ~30 minutes
Test 2 ~1200°C for ~30 minutes
Test 3~1200°C for ~5 minutes

ARTHUR LAKES LIBRARY
COLORADO SCHOOL OF MINES
GOLDEN, CO 80401

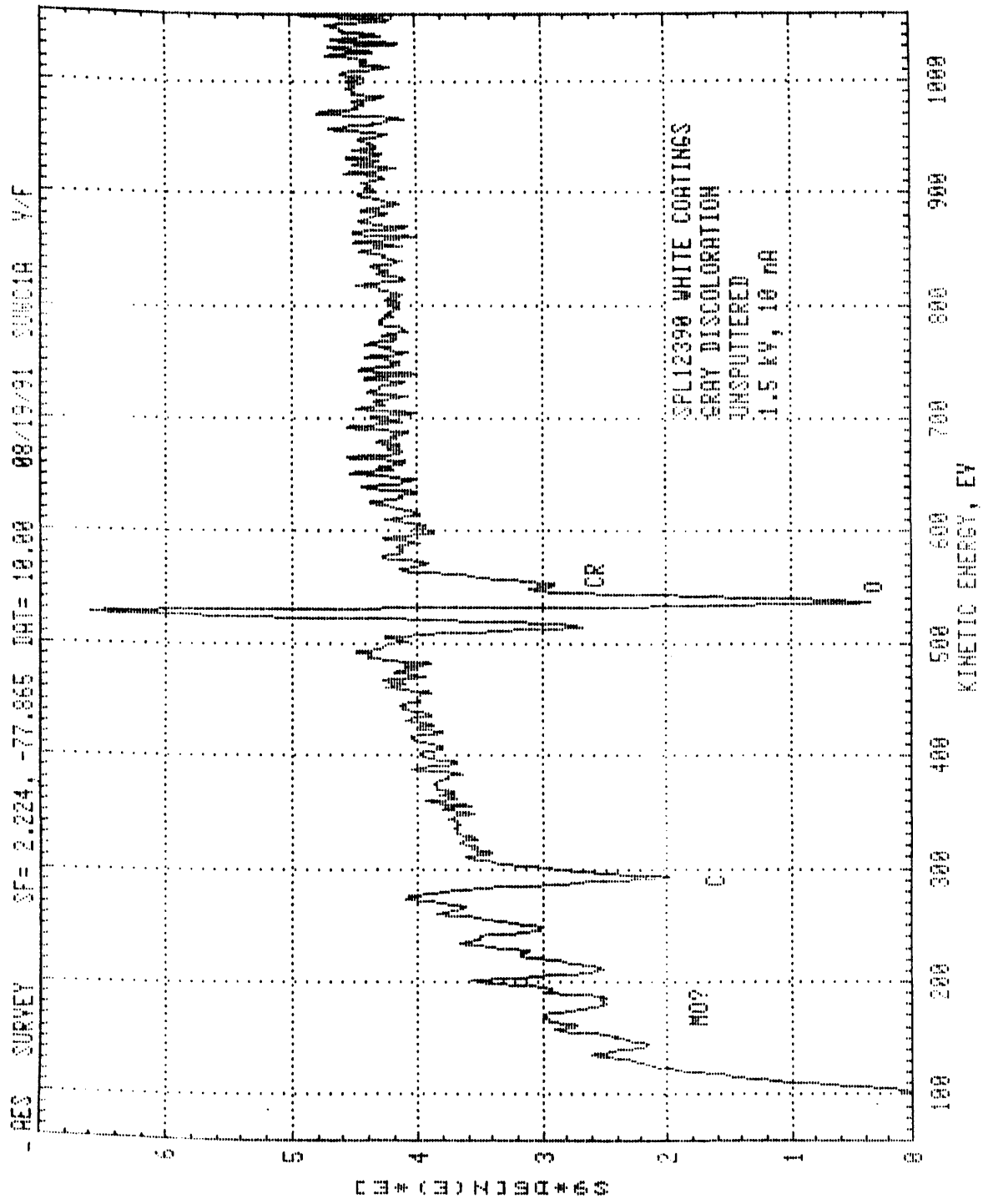

Figure 22 Auger Spectrum of HT-1

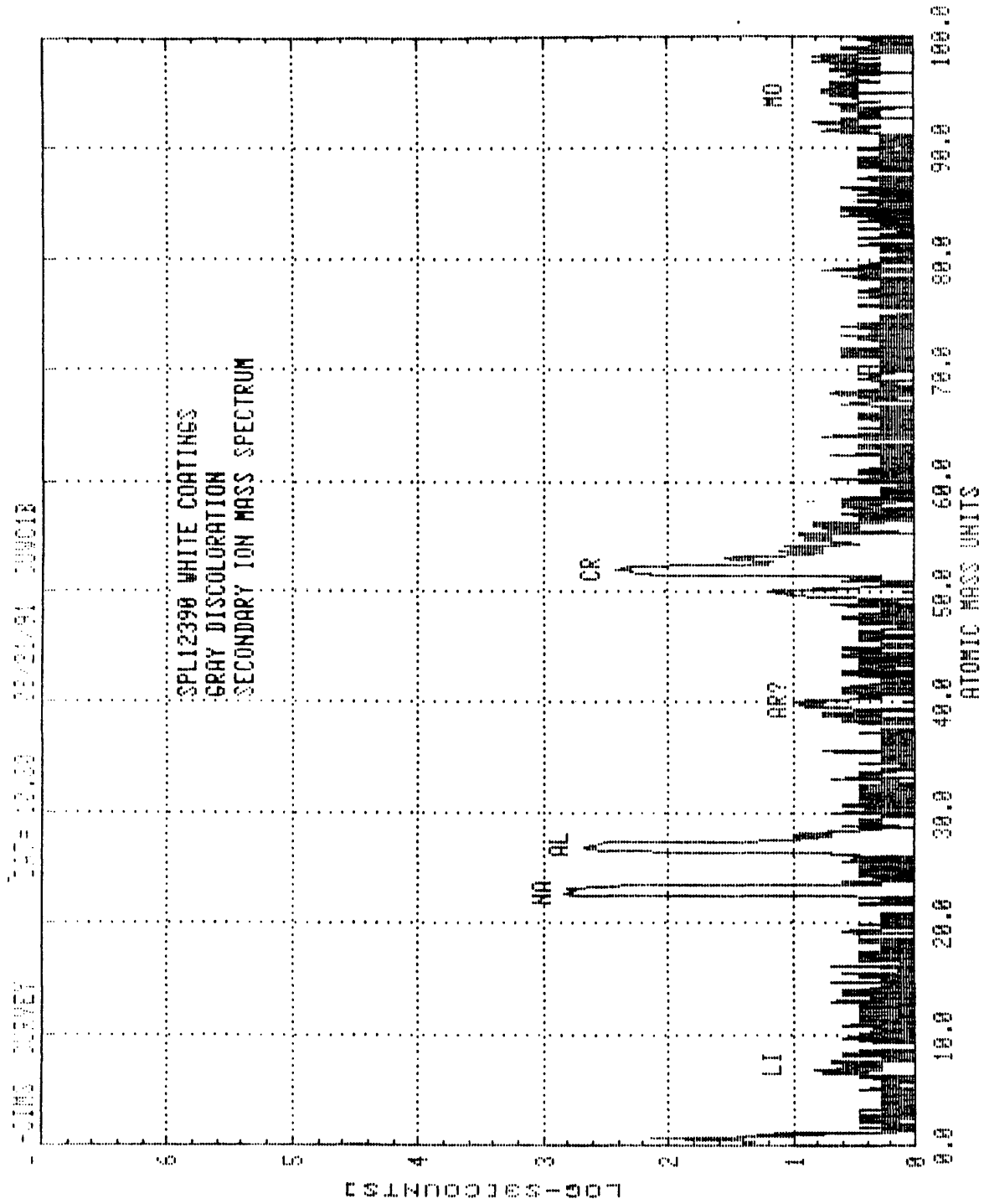

Figure 23 SIMS Spectrum of HT-1

An additional EDX was performed on an area of the coating which had been scraped to remove the gray surface discoloration, leaving a yellowish discoloration underneath. This spectrum is shown in Figure 25. This analysis shows the presence of manganese (Mn) and Fe and the absence of Cr.

4.4.2 Heat Treatment Test 2

Sample HT-3 exposed to ~1200°C for ~30 minutes (without precleaning of the coated side or backside) without other samples present in the furnace. This sample emerged with a noticeable yellowish discoloration. An additional EDX was performed, and again the presence of Cr, Mn, and Fe were observed. This spectrum is shown in Figure 26.

4.4.3 Heat Treatment Test 3

A pre-heat treatment EDX was performed on HT-4 to establish whether detectable amounts of Cr, Mn, or Fe were inherently in the coating, prior to baking. This spectrum is shown in Figure 27.

BA200 samples HT-4 and HT-5 were then exposed to ~1200°C for ~5 minutes while contained in an alumina crucible. Substantial whitening (lower α_s) was observed on HT-5 while no change was observed HT-4. Pre and post heat treatment UV-Visible reflectance scans, Figure 28, were performed on HT-4. In these spectra, a significant increase in reflectance in the near-IR region (~2μm) is apparent, however only a minimal increase in solar absorptivity results. This is due to the low contribution of the weighting factors in this region used to calculate the solar absorptivity.

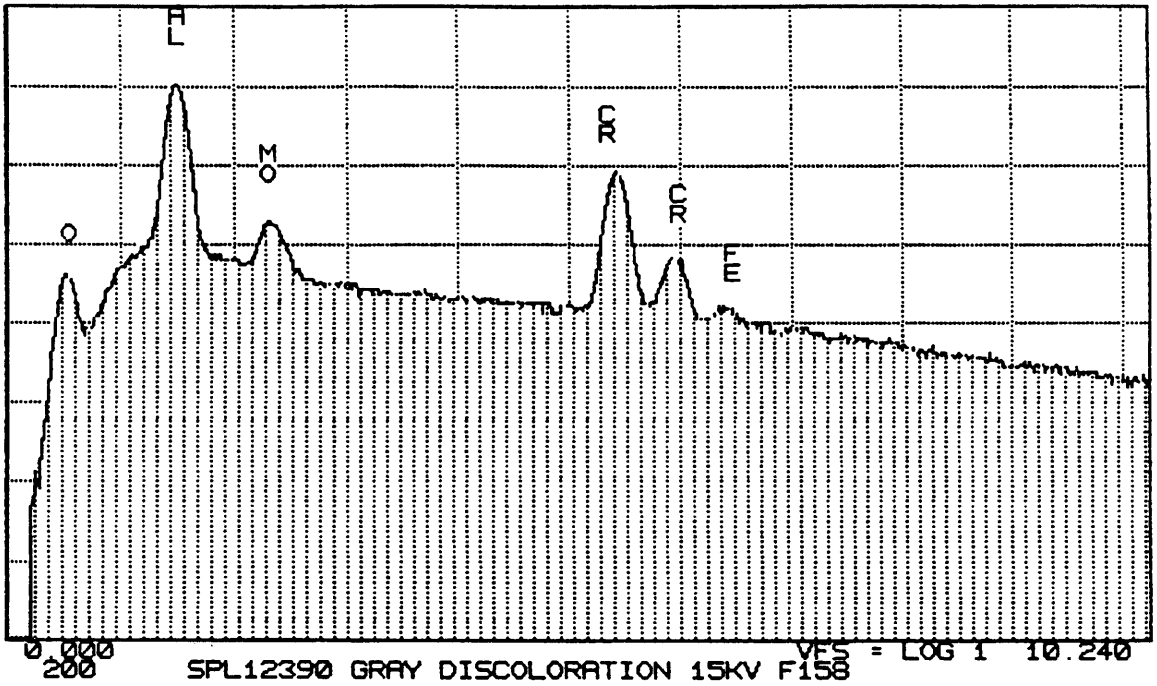

Figure 24 EDX Spectrum of HT-1

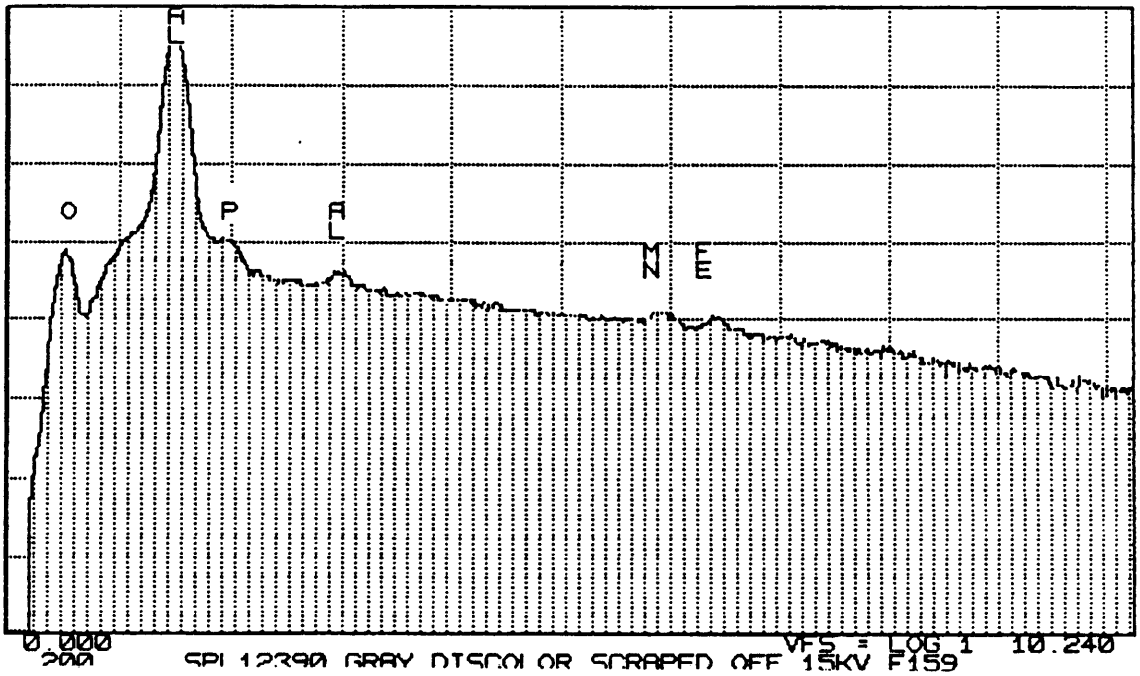

Figure 25 EDX Spectrum of Lighter Area on HT-1

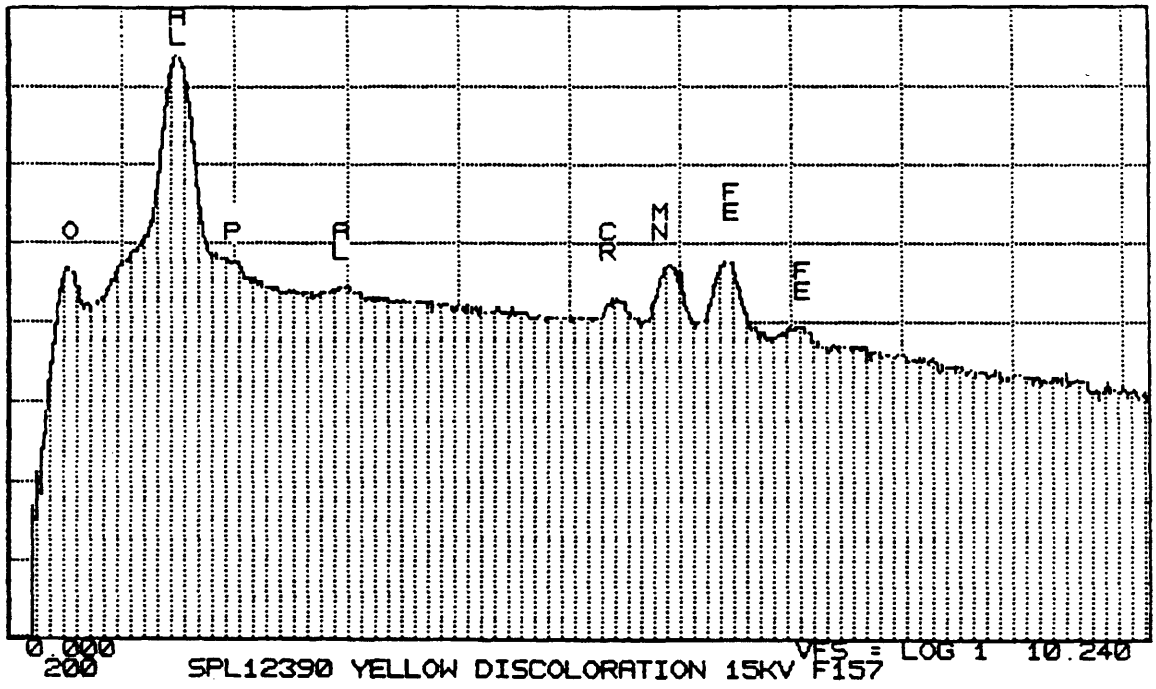

Figure 26 EDX Spectrum on HT-3

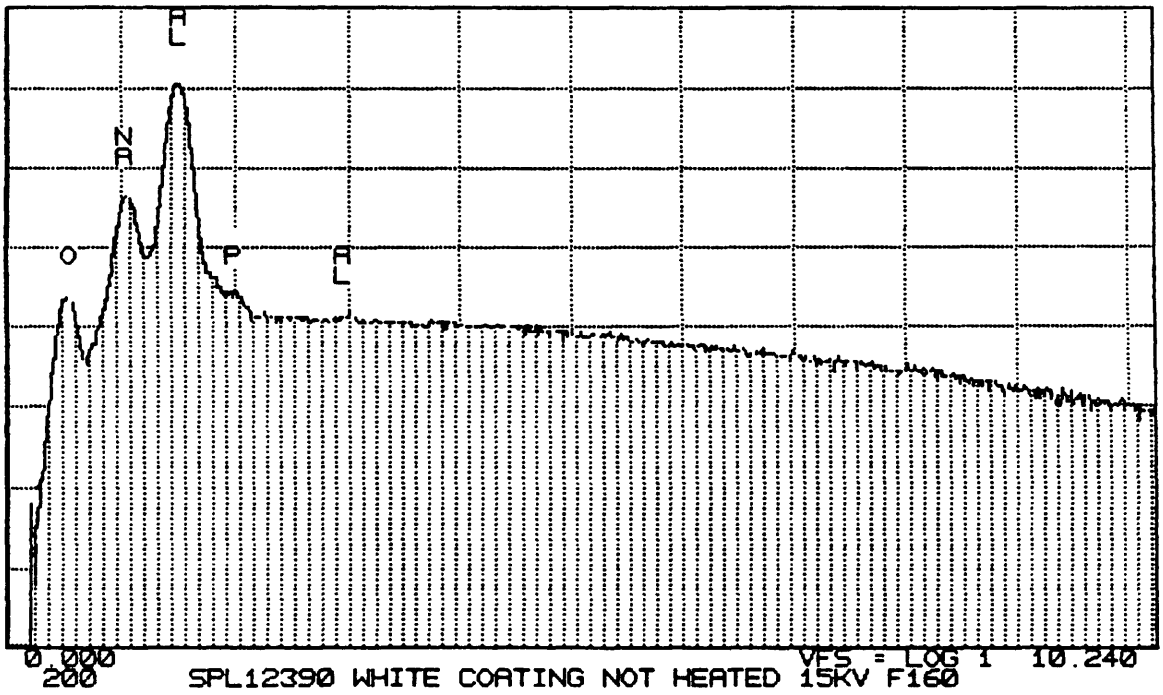

Figure 27 Pre Heat Treatment EDX Spectrum on HT-4

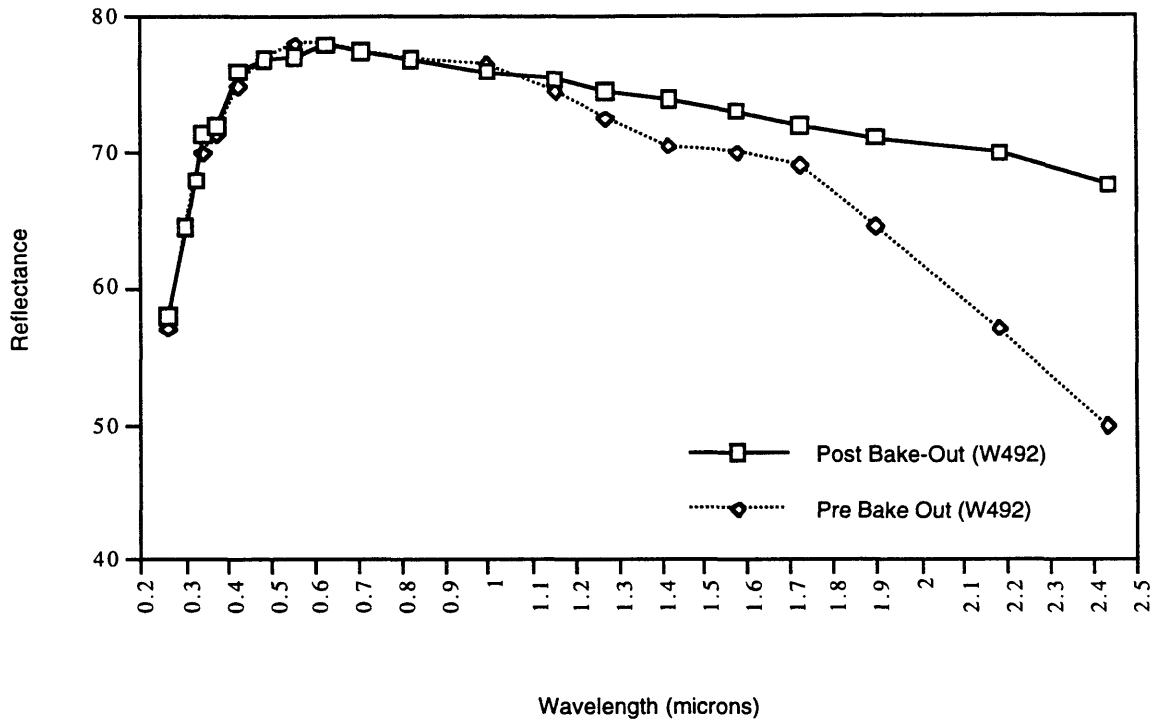

Figure 28 Pre and Post Heat Treatment UV-Vis Reflectance Spectra on HT-4

The first two test series of samples exposed showed severe coating discoloration. The third series of samples exposed showed a noticeable decrease in the α_s of one sample and no visible change on the other sample. The samples in the first two test series were exposed " as is". The samples of the third test were polished on the backside (Mo side) to remove markings and oxidation scale from the plasma spaying process. The source of the contamination in the first two tests was not been identified, but is assumed to have either come from the backside of the coupons or the furnace. The samples in the first two tests were heated in the directly in the furnace chamber while in the third test they were heated in alumina crucibles.

4.5 Surface Resistivity.

Surface resistivity of the BA200 coating was measured in accordance with ASTM D-257. Results of these measurements are contained in Table 14.

Table 14 ASTM D-257 Surface Resistivity of BA200 Coatings

(ungaurded)	1.1×10^8 ohm•cm
(Using conductive rubber pads)	3.7×10^7 ohm•cm

4.6 Ultraviolet and Electron Exposure Stability.

Ultraviolet and electron stability of the BA200 coating, as well as other white thermal control coatings, were characterized. Control samples were tested to correlate optical property degradation with space flight experiments. Control samples (Optical Solar Reflector (OSR), Silverized Teflon, YB71, Z93, S13G/LO, and Chemglaze A276) were run to compare the laboratory exposure results with Long Duration Exposure Facility (LDEF) space flight experimental data.[21, 37, 38] Results of the ultraviolet and electron irradiation testing are shown in Table 15. Test conditions for the Ultraviolet stability characterization are shown in Table 16.

Table 15 Ultraviolet and Electron Exposure Results

Coating	PreTest		Post Test			LDEF Degradation
			VUV-NUV		e^-	
	α_s	ε_h	α_s	ε_h	$\Delta\alpha_s$	
BA200, undoped (c)	0.18	0.89	0.21	0.90	0.03	Not Applicable
SFP 105, (a)	0.21	0.81	0.27	0.81	0.08	Not Applicable
BA200 Ce_2O_3 doped (c)	0.22	0.88	0.26	0.90	0.03	Not Applicable
BA200 Ce_2O_3 doped (c)	0.23	0.88	0.26	0.88	0.05	Not Applicable
OSR, Ag 5mil, (a)	0.08	0.79	0.09	0.79	0.01	$\Delta 0.03\ \alpha_s / \Delta 0.0 \varepsilon_h$
Ag Teflon, (a)	0.08	0.79	0.10	-	0.05	$\Delta 0.02\ \alpha_s$
YB71, (a)	0.13	0.89	0.19	0.89	0.04	$\Delta 0.07\ \alpha_s / \Delta 0.00 \varepsilon_h$
Z93, (a)	0.14	0.92	0.17	0.92	0.02	$\Delta 0.02\ \alpha_s / \Delta 0.01 \varepsilon_h$
S13G/LO, (a)	0.17	0.90	0.21	0.89	0.06	$\Delta 0.33\ \alpha_s / \Delta 0.01 \varepsilon_h$
A276, (b)	0.24	0.89	0.41	0.89	-	$\Delta 0.3\ \alpha_s / \Delta 0.03 \varepsilon_h$

Exposures:
(a) VUV;1000Equivalent Sun Hours (ESH), NUV;500 ESH, e^-;~10^9 rads
(b) VUV;400Equivalent Sun Hours (ESH), NUV;300 ESH, no e^- exposure
(c) VUV;1000Equivalent Sun Hours (ESH), NUV;400 ESH, e^-;~10^9 rads
The OSR and Ag Teflon samples are control samples tested to show a correlation to LDEF flight experiments (See section 4.6). The YB71, Z93, S13G/LO, and A276 samples are current white thermal control materials (see Section 2.1.1) which were also flown on LDEF experiments(see Section 4.6).

Table 16 Ultraviolet Stability Characterization Test Conditions

Pressure	10^{-6} torr vacuum
Visible Ultraviolet Irradiation, (0.15- 0.18 μm), Xenon Lamp (low pressure)	2X Suns
Near Ultraviolet Irradiation, (0.25 - 0.40 μm) Xenon Lamp (high pressure) Xenon Lamp (high pressure)	2X Suns
In-Situ Spectral Reflectance	0.25 - 2.5 μm

5. CONCLUSIONS

Plasma-sprayed BA200 coatings are a comparable alternative to existing spacecraft coatings offering several advantages. The BA200 coatings offer exceptional durability in the manufacturing environment requiring less maintenance during the spacecraft assembly. The cost of the BA200 coating is comparable to current thermal control coatings. The surface conductivity properties of the BA200 coating are desirable for triboelectric charge dissipation. Although it is apparent from this investigation that more research is needed to optimize and characterize the BA200 coatings for spacecraft thermal control surfaces, the BA200 coatings have space stability comparable to the current coatings used.

Several conclusions can be drawn from the plasma-spray optimization data. The optimum power setting of 37.5 kW showed consistently lower absorptivities, when all other variables (including thickness) remained constant. Most importantly it is apparent that thicker coatings show a lower α_s no matter which variable was optimized. The number of spray cycles to reach a desired thickness is influenced by the powder feed rate. Higher feed rates appear to result in lower α_s values, but this appears to be the result of the thicker coatings produced. It should be considered that the number of spray cycles and feed rate directly influence the thickness and deposition rate (mils/cycle) and that no apparent correlation on what the optimum feed rate and deposition rate or their interrelationships can be concluded from the data. Coating thickness of greater than 10 mils show consistent values of α_s lower than 0.25. Variations of the α_s can probably be attributed to the influence of uncontrolled variables in the of the plasma spray process, and are probably just statistical variation.

Further designed experimentation needs to be performed to understand the individual interrelationships of the plasma spraying variables upon the α_s in order to further optimize the BA200 optical properties. A design of experiments (DOE) approach would prove useful in understanding the interdependencies of the plasma-spray variables.

A more thorough characterization effort (microstructure and chemistry) of the optimized coating will lead to the understanding what physical properties (e.g., density, porosity, grain size, etc.) are influencing the α_s, which will lead to more results.

Examination of the XRD data shows that there is some phase transformation occurring during the plasma-spray process. The major conclusion reached from the coatings examined was that they all predominantly matched α-Al_2O_3. (JCPDS file 10-173). The sodium aluminum compound found in the BA200 powder (JCPDS file 38-36, $Na_{17}Al_5O_{16}$) was a different phase than found in the resultant coatings (JCPDS file 19-1173, $NaAl_5O_8$. Of an interesting note was the evidence of γ-Al_2O_3 (JCPDS file 10-425) in a heat treated sample, which corresponded to a low α_s (0.18)

From examination of the heat treatment data it is apparent that vacuum baked samples may result in lower BA200 coatings α_s, if contamination is not present. Two samples were exposed to ~1200°C for ~5 minutes and one exhibited a significant reduction in the α_s. Contamination from either the vacuum chamber used to heat the initial samples or from the sample itself resulted in the severe discoloration in the coating. None of the elements (Cr, Fe, Mn) found on the discolored samples were found in the initial coatings. As

a consequence it is very apparent that small amounts of elemental contamination will result is severely discolored coatings (increased α_s.)

During this investigation, the surface resistivity of the BA200 coatings were measured. This was initiated due to electrical conductivity properties of sodium aluminate used in solid state electrolyte batteries. The result of this testing showed that the BA200 coatings are somewhat conductive and meet the spacecraft coating requirements for triboelectric charging.

BA200 coatings show comparable ultraviolet stability to existing spacecraft thermal control coatings when tested under laboratory simulated environments. BA200 samples doped with Ce_2O_3 showed equivalent degradation as compared to the undoped sample. The doping of the initial BA200 powder probably was ineffective in preventing color center formation for these experiments. This was probably due the doping technique (grinding the two powders together) and the low calcination temperature (~1000C) to allow the Ce^{+3} ions to be homogeneous in the resultant powder..

Costs associated with the application of plasma-sprayed thermal control coatings have been estimated. These costs, as well as the costs associated with the application of the current spacecraft thermal control coatings are shown in Table 17.

Table 17 Comparison of Thermal Control Coatings

Name	density (g/cc)	Thickness (mil)	$ /pint	ft^2 /pint	$ /ft^2	grams/ft^2
A276	1.2	5	15	30	0.5	14
S13G/LO	1.5	5	500	30	16.67	18
92-007	1.5	5	10	28	0.357	18
YB-71	2.5	8	950	4	237.5	47
Z-93	2.1	5	125	4	31.25	25
MS-74	3.5	4	600	4	150	33
BA200			NA	NA	150	

6. REFERENCES

1 Triolo,J.J., Heaney,J.B., Hass,G., "Coatings in Space Environement", SPIE Vol. 121, Optics in Adverse Environments, p46-66, 1977

2 Zerlaut,G.A., Gilligan,J.E., Ashford,N.A., "Space Radiation Effects in Reactively Encapsulated Zinc OrthoTitanates and Their Paints", AAIA 6th Thermophysics Conference, AIAA Paper 71-449, 1971

3 Saylor,W., Racette,G., Singh,B., Amore,L., "Evaluation of Thermal Control Surface On-Orbit Servicing Methods For Long Term Missions", AAIA 20th Thermophysics Conference, AIAA Paper 85-0956, 1985

4 Ahern,J.E., Karperos,K., "Calormetric Mesurements of Thermal Control Surfaces on Operational Satellites", AIAA 21st Aerospace Sciences Meeting, AIAA Paper 83-0075, 1983

5 Harada,Y., Mell,R.J., Wilkes,D.R., "The Effect of the Space Environment on Thermal Control Coatings", SPIE Vol. 1330, Optical Surfaces Resistant to Severe Environments, 1990

6 Mossman,D.L., Barsh,M.K., Greenberg,S.A., "Ultraviolet and Electron Irradiation of DC-704 Oil on Zinc OrthoTitanate Paint", AIAA/ASME 3rd Joint Thermophysics, Fluids, Plasma and Heat Tranfer Conference, (82-0865), 1982

7 Stevens,N.J., Smolak,G.R., "Report on the Flight Performance of the Z-93 White Paint used in the SERT II Thermal Control System", AIAA 6th Thermophysics Conference, AIAA Paper 71-455, 1971

8 Papazian,H.A., "Solar Absorptance Changes of Thermal Control Coatings in Flight", AIAA Paper 84-0059, January 1984

9 "Thermal Control Coatings for High Thermal Conductivity Substrates", Lockheed Martin Technical Proposal P95-41344, 1995

10 Kramer,T.J., "Thermal Control Design and Performance of Air Force Satellite STP P72-1", ASME 77-ENAS-41, AIAA Paper A77-46882, 1977

11 Whitaker,A.F., Little,S.A., Harwell,R.J., Griner,D.B., DeHaye,R.F., "Orbital Effects on Thermal Control and Optical Materials", AIAA 23rd Aerospace Sciences Meeting, AIAA Papaer 85-0416, 1985

12 Spieth,B.D., "Basic Physics of Radiation Effects Due to Particle Interactions", Lockheed Martin Report, 1991

13 Hall,D.F., Fote,A.A., "α_s / ε_h Measurements of Thermal Control Coatings Over Four Years at Geosynchronous Altitude", AIAA Thermophysics Conference, AAIA Paper 83-1450, 1983

14 Campbell, William B., Cochran,Joe K., "Degradation Mechanisms of Pigmented Coatings", Air Force Materials Lab Technical Report, AFML-TR-71-42, 1972

15 Glass,A.M., Searle,T.M., "Reactions between Vacancies and Impurities in Magnesium Oxide.II.Mn^{4+}-Ion and OH^--Ion Impurities" Journal of Chemical Physics, Vol. 46, No. 6, p2092-2101, 15 March, 1967

16 Chon,T., Nerz,J.E., Kushner, Jr.,B.A., Rotolico,A.J., Riggs,W.L., "Design of Experiment Study of Plasma Sprayed Chromium Carbide/Nickel Chromium and Aluminum Oxide Coatings", Proceedings of the Fourth National Thermal Spray Conference, p3-11, 1991

17 Salsbury,R.L., "Quality Control of Hydroxylapatite Coatings: Purity and Crystallinity Determinations", Proceedings of the Fourth National Thermal Spray Conference, p471-473, 1991

18 Bosma,S.J., Levadou,F., "The Simulation of Ultra-Violet Irradiation Effects on Candidate Spacelab Thermal Control Coatings", AIAA Paper A79-10591, 1978

19 Smith, James A., "Apollo 9 Thermal-Control-Coating Degradation", NASA TN D-6863 (N72-25864), 1972

20 Ahern,J.,E., Belcher,R.L., Karperos,K., Ruff,R.D., "Long Life Performance of Satellite Thermal Control Surfaces", Aerojet Technology, AIAA Paper A84-31808, 1984

21 Hurley,C.J., "Long Duration Exposure Facility Experiment M0003-5, Thermal Control Materials", LDEF-69 Months in Space, 1st Post Retrieval Symposium, NASA Conference Publication 3134, Part 2, pp 961f

22 Harada,Y., Mell,R.J., "Inorganic Thermal Control Coatings, A Review", AIAA 21st Aerospace Sciences Meeting, AIAA Paper 83-007, 1983

23 Schulman,James H., Compton,W. Dale, Color Centers In Solids, The MacMillan Company, New York, p1-2, 1962

24 Pankove,J. I., Optical Processes in Semiconductors, Dover Press, NY, 1971.

25 Schulman, p38-39, 214

26 Schulman, p212

27 Schulman, p213

28 Schulman, p214

29 Schulman, p228

30 Schulman, p226

31 Schulman, p175

32 Schulman, p169

33 Schulman, p41

34 Swalin,Richard A., Thermodynamics of Solids, John Wiley & Sons, New York, 1972, p261

35 Lockheed Martin, Internal Research and Development Program (IRAD) D-66D, 1990, 1991

36 Metco, A Divion of Perkin Elmer

37 Hurley, C.J, LDEF Materials Workshop '91', pp19-22, November 1991

38 Wilkes,D.R., et. al., "Initial Materials Evaluation of the Thermal Control Surfaces Experiment (S0069)", NASA Conference Publication 3134, Part 2, pp 899f.